

**Design of a Wearable Ultrasound Doppler Sensor to Monitor Blood  
Flow in the Common Carotid Artery**

by

**Elie Awad**

B.S.M.E., American University of Beirut - Lebanon, 1997

Submitted to the Department of Mechanical Engineering in Partial Fulfillment of the  
Requirements for the Degree of

**MASTER OF SCIENCE IN MECHANICAL ENGINEERING**

at the

**MASSACHUSETTS INSTITUTE OF TECHNOLOGY**

June 1999

© 1999 Massachusetts Institute of Technology  
All rights reserved

Signature of Author \_\_\_\_\_

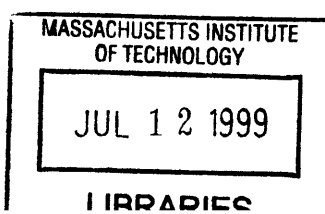
Department of Mechanical Engineering  
May 7, 1999

Certified by \_\_\_\_\_

Haruhiko H. Asada  
Ford Professor of Mechanical Engineering  
Thesis Supervisor

Accepted by \_\_\_\_\_

Ain A. Sonin  
Chairman, Department Committee on Graduate Students



Eng.

# **Design of a Wearable Ultrasound Doppler Sensor to Monitor Blood Flow in the Common Carotid Artery**

by

**Elie Awad**

Submitted to the Department of Mechanical Engineering in Partial Fulfillment of the  
Requirements for the Degree of

**MASTER OF SCIENCE IN MECHANICAL ENGINEERING**

## **Abstract**

A novel design for a wearable and non-invasive ultrasound Doppler blood flow measuring device is presented. The device consists of an array of piezoelectric transducers that mount at the neck and generate different ultrasonic beams directed at the common carotid artery. The Doppler frequency shift generated by the moving blood is then processed to reconstruct the centerline velocity of the artery as well as to provide an estimate of the velocity profile and other physiological parameters. The presented design covers key issues relevant to making this technology wearable mainly handling the location uncertainty of the artery and interpreting the measurement without human assistance with the restriction of keeping the technical complexity of the device low for all cases.

The array of transducers is designed to enable the coverage of a wide sector in the neck that encompasses the artery. Different beams can be produced by the array depending on the number of transducers that are excited. The centerline velocity of the artery is used as a criterion to decide which transducers are favorably oriented and hence should be operated. Novel algorithms to process the received signal to estimate the velocity profile and the time derivative of pressure are presented.

The thesis builds upon theoretical analysis and includes computer simulation and experimental verification of the key ideas.

**Thesis Supervisor:**

Haruhiko H. Asada

Ford Professor of Mechanical Engineering

# Table of Contents

<b>ABSTRACT .....</b>	<b>2</b>
<b>TABLE OF CONTENTS .....</b>	<b>3</b>
<b>LIST OF FIGURES .....</b>	<b>5</b>
<b>1 INTRODUCTION.....</b>	<b>7</b>
1.1 OBJECTIVE AND SCOPE .....	7
<b>2 THE DOPPLER NECKLACE.....</b>	<b>10</b>
2.1 SITE SELECTION .....	10
2.2 GENERAL DESCRIPTION .....	11
<b>3 BLOOD FLOW IN THE COMMON CAROTID ARTERY.....</b>	<b>14</b>
3.1 FLOW PHYSICS .....	14
3.1.1 <i>Reynolds Number</i> .....	14
3.1.2 <i>Poiseuille Flow</i> .....	15
<b>4 DESIGN OF THE DOPPLER NECKLACE.....</b>	<b>18</b>
4.1 OPERATING PRINCIPLE.....	18
4.2 SELECTION OF OPERATING MODE: CONTINUOUS VS PULSED .....	19
4.3 DETERMINATION OF OPERATING FREQUENCY .....	20
4.4 MOUNTING ANGLE .....	21
4.5 LOCATION UNCERTAINTY OF THE ARTERY .....	22
4.5.1 <i>Using a Single Large Transducer</i> .....	23
4.5.2 <i>Diverging Beam</i> .....	24
4.5.2.1 Transducer with Convex Lens.....	24
4.5.2.2 Using Curved Transducers.....	26
4.5.2.3 Limitations.....	26
4.5.3.1 Mode of Operation: Phased Array vs Switching .....	27
4.5.3 <i>Design of the Emitting Transducers</i> .....	29
4.5.3.1 Vertical Dimension of Emitting Transducers.....	29
Velocity Resolution.....	29
Angle Uncertainty .....	31
4.5.3.2 Horizontal Dimension and Spacing of Emitting Transducers.....	33
4.5.4 <i>Receiving Transducers</i> .....	33
4.6 TRANSDUCER SELECTION AND MOUNTING .....	34
4.7 ATTACHMENT TO SKIN .....	35
<b>5 INTERPRETATION OF THE SIGNAL.....</b>	<b>39</b>
5.1 MONITORING BLOOD VELOCITY ALONG THE CENTERLINE.....	39
5.1.1 <i>Finding <math>F_{max}</math> as Energy Envelope</i> .....	40
5.1.2 <i>Finding <math>F_{max}</math> by Setting Threshold</i> .....	40
5.2 ESTIMATING FLOW AND VELOCITY PROFILE .....	40
5.2.1 <i>Zero-Cross</i> .....	42
5.2.2 <i>Spectral Analysis of the signal</i> .....	43
5.2.2.1 First moment of Area .....	43
5.2.2.2 Mean Velocity and Flow Profile .....	43
5.2.3 <i>Effect of Acoustic Distribution</i> .....	44
5.2.3.1 Beam Formation.....	44
5.2.3.2 Beam Uniformity .....	46

Operating around the onset of the far field .....	47
‘Speckle effect’ .....	47
5.2.3.3 Accounting for Beam Nonuniformity .....	48
5.3 WALL MOTION .....	50
5.4 CAROTID FLOW AS INDEX OF DIASTOLIC CEREBRAL FLOW .....	55
<b>6 EXPERIMENTAL RESULTS AND COMPUTER SIMULATIONS.....</b>	<b>57</b>
6.1 OVERALL SETUP.....	57
6.2 SIMULATING THE ULTRASONIC FIELD DISTRIBUTION .....	57
6.2.1 <i>Field for an Individual Crystal</i> .....	58
6.2.2 <i>Field Generated by a Convex Tranducer</i> .....	58
6.2.3 <i>Field Uniformity</i> .....	58
6.2.4 <i>Multiple Emitters</i> .....	59
6.2.5 <i>Multiple Receivers</i> .....	60
6.3 TRACKING THE CENTERLINE VELOCITY .....	61
6.4 ESTIMATING VELOCITY PROFILE ASSUMING UNIFORM INSONIFICATION .....	61
6.5 ESTIMATING VELOCITY PROFILE BY ACCOUNTING FOR NON-UNIFORMITY OF INSONIFICATION .....	62
6.5 WALL VELOCITIES.....	64
<b>7 CONCLUSION .....</b>	<b>72</b>
<b>APPENDIX: BASIC ULTRASOUND INFORMATION .....</b>	<b>73</b>
PROPAGATION .....	73
ATTENUATION.....	73
REFLECTION AND REFRACTION .....	74
BACKSCATTERING BY BLOOD CELLS.....	74
<b>REFERENCES.....</b>	<b>76</b>

## List of Figures

Figure 2.1: Anatomical views.....	12
Figure 2.2: Diagrammatic representation of a continuous wave Doppler device.....	12
Figure 2.3: Schematic representation of Doppler Necklace .....	13
Figure 3.1: Measured blood flow velocity distribution in the common carotid artery. (A) systole (B)late diastole (C) mid-diastole (D) late diastole.....	17
Figure 4.1: Coordinates adopted to reference the transducers to the neck .....	37
Figure 4.2: Setup used by Matsumoto et al (1989) to take continuous measurements at the common carotid artery consisted of two 15mm semicircular transducers.....	37
Figure 4.3: parameters of the acoustic lens.....	37
Figure 4.4: driving the transducers with a delay creates a ‘steering’ effect by generating different wavefronts.....	38
Figure 4.5: The ideal mounting arrangement for the Doppler Necklace array: the individual crystals are airbacked and ‘glued’ to the skin with a proper acoustic coupling medium.....	38
Figure 5.1: Doppler frequency spectrum shown as cell count vs cell velocity plot. ....	56
Figure 5.2: Reference used in calculating the acoustic field distribution.....	56
Figure 5.3: variation of the magnitude of the on-axis pressure field from a circular transducer.....	56
Figure 6.1: intensity field for 2mm by 5mm transducer at CW excitation of 8.1 MHz....	65
Figure 6.2: simulated acoustic field for 5mm wide planar transducer.....	65
Figure 6.3: simulated acoustic field of a 5mm convex (diverging) transducer.....	65
Figure 6.4: simulated acoustic field for an array of 0.5 mm transducers spaced by 0.5 mm, note the ‘speckle’ effect in the region between 6 and 10 mm.....	66
Figure 6.5:simulated acoustic field of an array of 1mm wide transducers, note that the field irregularity is greater than that of figure 6.4 above.....	66
Figure 6.6: the ultrasound field for the proposed arrangement of 5 transducers of 2mm width each with 1mm between for the Doppler Necklace.....	67
Figure 6.7: Experimental setup to compare the range of coverage of multiple emitters vs a single emitter: the position of the emitters is varied while the receiver remains fixed. The crystals used are 2mm in width and spaced by 1 mm between.....	67
Figure 6.8: The result of the experimental setup of figure 6.7: the x-axis represents the lateral displacement in mm of the emitter and the y-axis is the voltage output of the zero cross detector. The use of two emitters provides wider coverage than the use of a single one.....	68
Figure 6.9: Spectrogram of the Doppler reading from the common carotid artery with the maximum velocity estimated to hold 98% of the energy of the useful signal within it.....	68
Figure 6.10: Velocity profile in the common carotid artery as reconstructed from the Doppler reading.....	69
Figure 6.11: Computer simulations for the new algorithm to calculate p.....	69
Figure 6.12: The theoretical power distribution for blunt profiles ( $p>2$ ) show a peak in the vicinity of $F_{max}$ . The higher the p, the more pronounced the peak. The figure above is for $p=4$ .....	70

Figure 6.13: Spectral distribution from the Doppler measurement shows the smearing effect close the region of $f = F_{max}$ .....	70
Figure 6.14 The measured value of the arterial wall velocity at the carotid artery is compared with an estimate based on substituting values from literature into equation 5.29 .....	71
Figure 6.15: upper plot shows the variation in the diameter of the common carotid artery (in mm) while the lower plot shows the pressure variation measured simultaneously at the brachial artery (from Hansen et al 1995).....	71

# **Chapter 1**

## **Introduction**

### **1.1 Objective and Scope**

Cardiovascular diseases are a prevalent cause of death in the contemporary society, and monitoring a patient's cardiovascular system is a critical part of today's healthcare system.

The current practice of continuous non-invasive monitoring of the cardiac state is through the use of ambulatory electrocardiogram (EKG) devices: electrodes are glued onto the chest of a patient and pick up the voltage signals that trigger the contraction of the heart muscles. EKG is thus a measure of a 'control signal' or input to the heart and Miyamoto et al. (1989) considered that it may not reflect the real functions of the heart as good as a measurement of blood flow. From a modeling perspective, the heart is not easily assessed by measuring its input alone because it behaves as a nonuniform and nonlinear combination of 'constant volume' and 'constant pressure' idealized pumps (Dinnar, 1983).

Blood pressure is another important variable of the cardiovascular state. It is one of the most useful diagnostic tools due to the empirical relations that have been established between blood pressure parameters and pathological conditions. However, pressure is not a better index for diagnosis than volumetric flow rates (Dinnar). The more widespread adoption of the former is mainly due to the fact that clinical procedures to measure it were developed earlier and are less complex than the latter. In fact, the occlusive cuff method of measuring systolic and diastolic blood pressure was first introduced by Riva-Rocci in 1896 (Chia, 1992) while measuring blood velocities using

continuous wave ultrasound Doppler was first suggested more than half a century later by Satomura in 1957 (Jensen 1996). Interestingly, pressure measurement has found its way into home healthcare while ultrasound diagnosis has strictly evolved within the hospital environment: current devices are highly sophisticated and often combine velocity measuring capabilities with real time imaging of the heart or the blood vessels.

Adapting the ultrasound technology to home healthcare poses the unique issue of eliminating the need for human assistance while keeping the technical complexity (and hence cost) low. In a hospital, human assistance plays a dual role of operating the ultrasound equipment and analyzing the measurements. The general motivation of our research is to design an easy-to-use wearable Doppler sensor in which the ultrasound transducers are secured to the skin of the patient and a reliable measurement is possible despite motion and location uncertainty of the target vessel. In addition, the sensor transmits the measurement to a computer that would analyze it in a continuous and systematic way.

The device described in this thesis and referred to as the ‘Doppler Necklace’ aims at monitoring blood flow in the common carotid artery which reflects both cardiac performance (Matsumoto et al. 1992) as well as diastolic cerebral flow (Champagne et al 1980). Different design issues that are unique to the device are addressed namely: handling the location uncertainty of the vessel, arranging the array of piezoelectric crystals, attaching the transducers to the skin and others. In addition to that, this thesis presents novel ideas in interpreting the signal. The arterial wall velocities picked up by the sensor are shown to relate to the time rate of change of the pressure pulse waveform. Also, the spectral distribution of the measurement is interpreted using both existing and

new approaches to reconstruct the velocity profile in the carotid artery and potentially calculate a dimensionless estimate of absolute flow without the need of measuring the vessel area.

The Doppler Necklace with its ability to monitor the different variables mentioned earlier will have a great impact in healthcare practice. In addition, it will open new opportunities on the research level because the measurement taken with the Doppler Necklace can be combined with other simultaneous physiological measurements. This enables a better understanding of the human cardiovascular and thermoregulatory system.

In terms of practical applications, the Doppler Necklace is not limited to cardiovascular monitoring but other potential uses also exist. One such application is for the early detection of small amounts of dissolved gas bubbles in the blood stream that give rise to characteristic high pitched ‘scratching’ signals in the ultrasound reading (Wells P.N.T. 1977) and that can prove fatal if untreated.

## **Chapter 2**

### **The Doppler Necklace**

The process of designing a wearable ultrasound Doppler sensor starts by selecting an appropriate anatomical site to perform the measurement. The section below states the reasons for choosing the common carotid artery and is followed by an overview of the Doppler Necklace itself.

#### **2.1 Site Selection**

In principle, the ultrasound Doppler technology can be adapted to measure the blood velocities in basically any artery (for example the digital artery, aorta...). However, the carotid artery was chosen because it has the following advantages over other sites:

1. The carotid artery is a main non-peripheral vessel. The left common carotid artery branches right up from the aortic arch (figure 2.1) while the right common carotid artery branches off from the Brachiocephalic trunk. It is thus representative of the cardiovascular state. In fact, Matsumoto et al (1992) have observed a good linear correlation between cardiac output and the blood flow volume in the common carotid artery.
2. The common carotid artery branches off into two vessels (figure 2.1). The inner branch (inner carotid artery) together with the vertebral artery provide the supply of blood to the brain. Matsumoto et al. (1992) had used the common carotid artery flow as an index of cerebral flow. Champagne and Farget (1980) had also reported that

during the diastolic phase, flow in the common carotid artery almost equals that in the inner carotid artery.

3. The common carotid artery lies at a rather shallow depth (figure 2.1) and is easily accessible with ultrasound. It also exhibits straightness and has minor secondary velocity components.
4. Aesthetically, the transducers (that emit and receive the ultrasound) can be incorporated within a necklace or other form of pendant at the neck.

## 2.2 General Description

The Doppler Necklace is basically a continuous wave (CW) Doppler system in which a sinusoidal voltage excites a piezoelectric crystal to create an ultrasonic beam. The beam intercepts the target vessel and its interaction with the moving blood cells gives rise to a frequency shift (the Doppler shift). The backscattered ultrasound carrying the Doppler shift is picked up by a receiving crystal and analyzed. A system employing two transducer crystals for transmitting and receiving ultrasound continuously is shown in figure 2.2 (from Jensen, 1996). The Doppler Necklace retains the same operating principle: its electronics hardware supplies a sinusoidal excitation to the emitting transducers and also separates the frequency shift in the received signal. However, the Doppler Necklace is unique in the way it handles location uncertainty: instead of a single emitter, it employs an array of transducers that mounts at the neck (at the level of the fourth or fifth cervical vertebra) and allows the generation of different wide ultrasonic beams to track the centerline of the carotid artery. The Doppler Necklace also transmits the information to a computer where it is analyzed. Figure 2.3 shows a schematic diagram of the device.

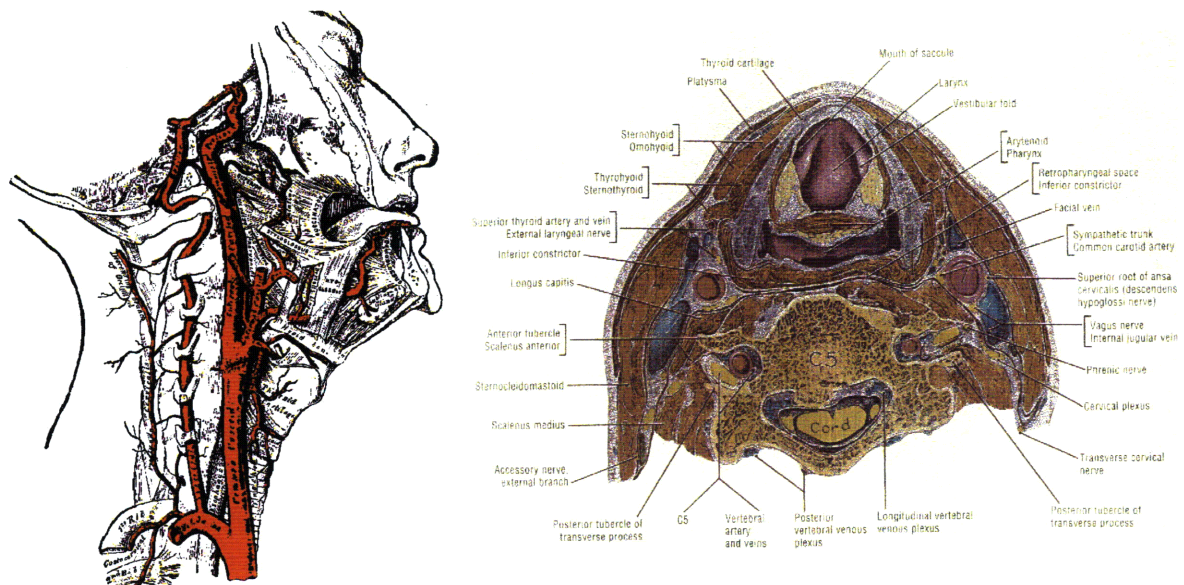
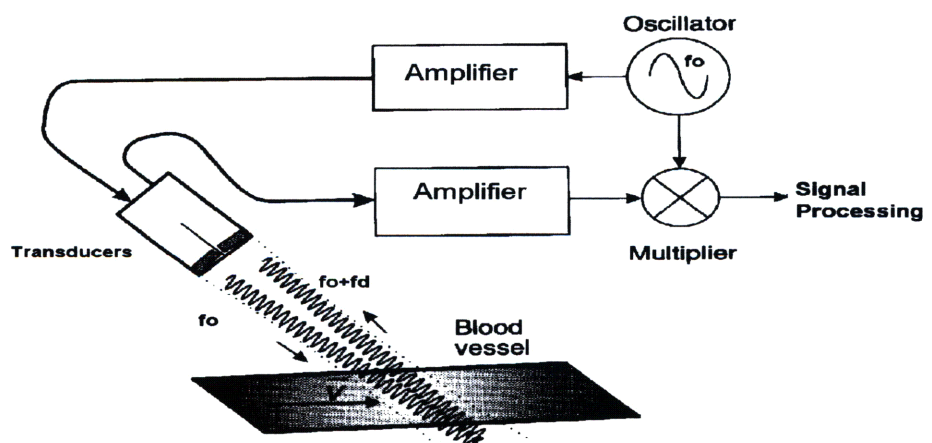


**Figure 2.1:** Anatomical views showing (left) the common carotid artery going up from the aortic arch and branching into inner and outer carotids (Gray's Anatomy). Right: A cross-section through the neck at the level where the Doppler necklace mounts (Grant's Atlas of Anatomy).



**Continuous wave Doppler system.**

**Figure 2.2:** Diagrammatic representation of a continuous wave Doppler device (Jensen 1996).

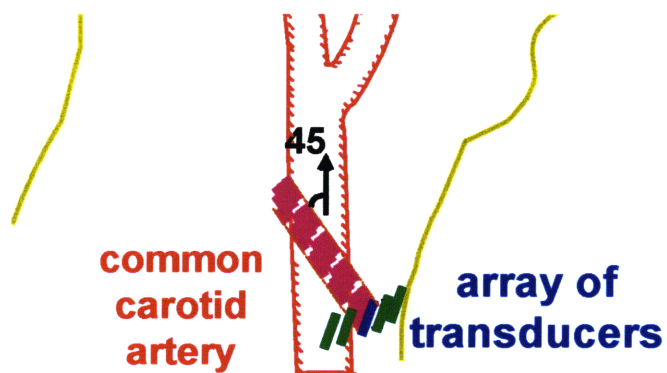
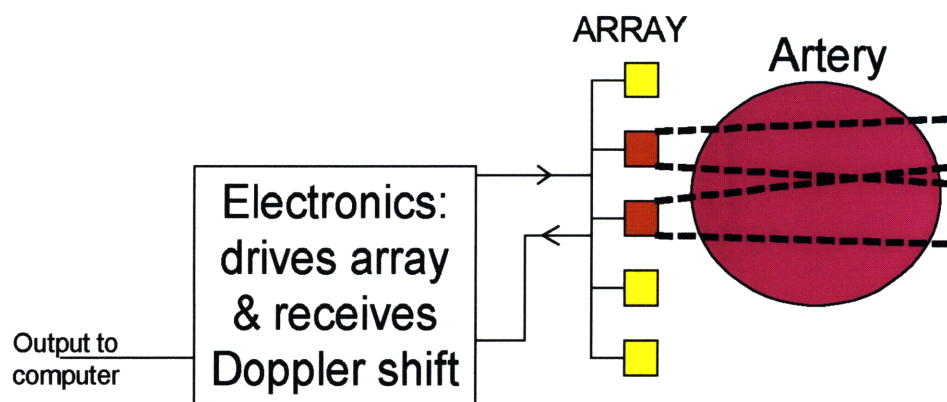


*Figure 2.3: A schematic representation of the Doppler Necklace*

## Blood Flow in the Common Carotid Artery

### 3.1 Flow Physics

The diameter of the common carotid artery in adults ranges from 0.2 to 0.8 cm with an average value of about 7mm (Arbeille 1997). A summary of typical dimensions and flow properties in the carotid artery and other main vessels is shown in table 3.1 from data taken by Caro et al (1974) and Brands (1995).

The common carotid artery just like other main arteries has a flexible wall that is thin compared to its diameter and that expands and contracts in response to the pressure pulsation. The flow can then be modeled as pulsatile flow in an elastic tube. Note that the most common vascular disease that evolves with age is the deposition of fat on the vessel walls. The fat could calcify with time and constrict the vessel leading to a hardened wall and an increase in blood velocities and possible onset of turbulence. The complex nature of the pulsatile flows that could evolve in the carotid artery under different conditions are difficult to model. Full description of the relationships between blood flow in the common carotid artery and the rest of the cardiovascular system is beyond the scope of this thesis and the following section will introduce some main features of carotid flow.

#### 3.1.1 Reynolds Number

A very important index in assessing the nature of a flow is the Reynolds number which for a circular tube is given by

$$Re = \frac{2R\rho}{\mu} V_{mean} \quad (3.1)$$

Where  $R$  is the radius of the tube,  $V_{mean}$  the spatial mean velocity and  $\rho$  and  $\mu$  the density and kinematic viscosity of the fluid. The Reynolds number is taken as an index in determining whether the flow is laminar or turbulent. It is assumed that the flow is laminar for  $Re < 2000$ . However, turbulence can occur at  $Re \sim 1000$  if the vessel wall is not smooth. For the common carotid artery, the maximum Reynolds number (at systole) is around 1850 and the flow can be considered laminar under normal conditions and in the absence of stenosis.

### **3.1.2 Poiseuille Flow**

Poiseuille flow describes the steady flow of a Newtonian fluid in a long tube of constant diameter. The velocity profile will be independent of the axial position along the tube and will only depend on the radial position  $r$  via a parabolic relationship given by:

$$v(r) = V_o \left( 1 - \left( \frac{r}{R} \right)^2 \right) \quad (3.2)$$

where  $V_o$  is the velocity at the centerline of the tube and  $R$  is the radius of the tube.

The Poiseuille equation for velocity distribution assumes that the tube is sufficiently long so that the flow has built up into a parabolic shape beyond the entrance region. In the circulatory system, and due to frequent vessel branching and pulsatility, the flow profile in the main arteries close to the heart changes over the cardiac cycle. The velocity distribution is better described by (Jensen 1996):

$$v(r) = V_o \left( 1 - \left( \frac{r}{R} \right)^p \right) \quad (3.3)$$

where  $p = 2$  for parabolic flow and  $p$  approaches infinity for a plug flow.

Several researchers have studied the variations of the flow index  $p$  over a cardiac cycle in the common carotid artery. Hein and O'Brien performed measurements on a phantom system with pulsatile flow and their results show almost parabolic profiles. In measurements performed in vivo, Miyamoto et al (1989) report more variations in  $p$  over the cardiac cycle: from being parabolic during diastole to a more blunt profile ( $p \sim 7$ ) at systole. Figures 3.1 shows a plot of the variations of the flow profile in the common carotid artery over time reported by Brands et al (1995).

Another important feature of the flow in the common carotid artery is the arterial wall elasticity. If the vessels were perfectly rigid, then any change in pressure at the heart would be propagated at the speed of sound throughout the vascular system. This is not the case because the elasticity of the vessel walls introduces a pressure propagation velocity. Typical pressure propagation speeds at the common carotid artery range between 0.6 and 1.1 m/s. Vessel wall motion is discussed again in Chapter 5.

Table 3.1: Typical dimensions and flows in vessels

Vessel	Internal Diameter cm	Wall thickness cm	Young's modulus $N/m^2 \cdot 10^6$	Peak velocity cm/sec	Peak Reynolds number
Ascending Aorta	1.0 - 2.4	0.05 - 0.08	3 - 6	20 - 290	4500
Carotid Artery	0.2 - 0.8	0.02 - 0.04	7 - 11	100*	1850 <sup>#</sup>
Femoral Artery	0.2 - 0.8	0.02 - 0.06	9 - 12	100 - 120	1000

Except where indicated, data is taken from Caro et al. (1974)  
 data is taken from Evans et al,  
<sup>#</sup> is an estimated value based on data from Evans and from Jensen

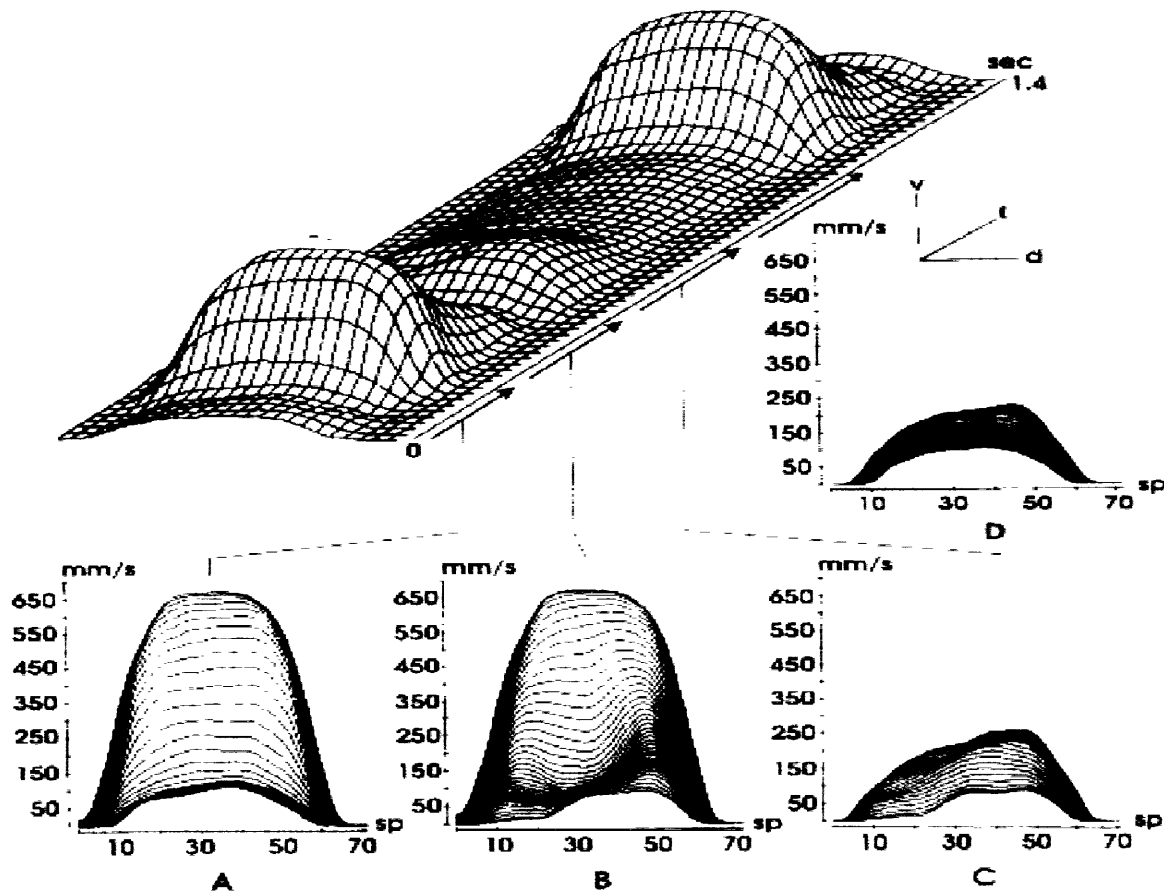


Figure 3.1: Measured blood flow velocity distribution in the common carotid artery. (A) systole (B) late diastole (C) mid-diastole (D) early diastole (Brands et al 1995).

## Chapter 4

### Design of the Doppler Necklace

#### 4.1 Operating Principle

The principle of operation of the device is the well-known Doppler effect: if a source moving at speed  $v_s$  is emitting a signal of a certain frequency  $f_o$ , a moving receiver will observe a frequency  $f_{obs}$  given by

$$f_{obs} = f_o \frac{c + v_o}{c + v_s} \quad (4.1)$$

where  $c$  is the speed of propagation of the signal in the medium and  $v_o$  the speed of the observer. In vascular ultrasonography, the beam intercepts the vessel and the blood cells act as receivers with respect to the emitting transducer and as emitters with respect to the receiving transducers so that the final frequency shift for one velocity component is given by (Jensen):

$$\Delta F = 2 \frac{f_o V \cos\theta}{c} \quad (4.2)$$

where  $V$  is the blood velocity,  $\theta$  the intercept angle and  $c$  the speed of sound in the medium.

The assumptions used in calculating  $V$  from the measured value  $\Delta F$  are that:

1. The speed of ultrasound in blood is constant at about 1560 m/sec.
2. The carotid artery runs parallel to the surface of the neck so that the angle of incidence of the beam can be set at 45 degrees by mounting the transducers accordingly (figure 4.1).

These two assumptions are common in traditional ultrasonic diagnostic tests and the error introduced by them is not serious for the case of the Doppler Necklace since patient monitoring is essentially a relative process rather than an absolute one.

## 4.2 Selection of Operating Mode: Continuous vs Pulsed

There are two modes of creating an ultrasound beam: one is continuous the other pulsed. In the continuous wave (CW) mode shown in figure 2.2, a sinusoidal voltage continuously excites a piezoelectric crystal to create an ultrasonic beam. The beam intercepts the target vessel and its interaction with the moving blood cells gives rise to the Doppler shift. The CW ultrasound is easy to implement but suffers from range ambiguity: the received signal carries information from all along the path of the beam. It is, therefore, quite possible that the received signal spectrum be distorted because of the beam intercepting two vessels located close to each others.

To achieve depth sensitivity, pulsed wave ultrasound can be used. A burst of pulses is emitted towards the vessel and since the speed of propagation  $c$  of the ultrasound is almost constant within human soft tissue, analyzing the signal received at a particular time corresponds to analyzing the signal backscattered from a particular depth. Note that pulsed systems are prone to aliasing when measuring high velocities and proper pulse repetition frequencies have to be selected.

The Doppler Necklace employs CW because the added complexity in implementing a pulsed wave system and its tracking system is not justifiable. On the contrary, information from all along the vessel is more important than localized information for our application.

### 4.3 Determination of Operating Frequency

In order to select the proper frequency to drive the transducers in the Doppler Necklace, a compromise has to be made between the absorption and the amplitude of the received signal, both of which increase with an increasing frequency. The attenuation of ultrasound in tissue has a linear dependence on frequency. On the other hand, the amplitude of the backscattered signal from red blood cells is a Rayleigh phenomenon and is dependent on the fourth power of the frequency (Appendix A).

In view of the above considerations, Reid and Baker (1971) have experimentally shown that for normal levels of blood hematocrit, the optimal frequency (in MHz) to be used for Doppler blood flow measurements is approximately given by [4]

$$f_{opt} = 90/d \quad (4.3)$$

where  $d$  is the thickness (in mm) of soft tissue between the vessel and the transducer face.

For the Doppler Necklace, the carotid artery lies at an approximate depth of 10 mm which gives a  $d$  of 14 mm (because of the 45° angle of insonification). The corresponding optimal frequency is about 6.5 MHz. However, Wells (1979) has pointed out that Reid and Baker did not take into account the increasing size of lower frequency transducers in their experiment and their equation provides an underestimation of the optimal frequency. Indeed Eriksen (1992) has used an 8MHz frequency to probe the common carotid artery and the equipment used in the experimental setup for the Doppler Necklace has an operating frequency of 8.1 MHz and provides a satisfactory result.

It is worth noting that other investigators have used lower frequencies for the carotid artery: Arbeille (1997) and Miyamoto (1995) used 4 MHz and 2 MHz respectively. This should be viewed in the light of availability of equipment for those

researchers rather than as a non-agreement on defining the optimal frequency. As a matter of fact, optimality is not an issue when energy consumption is not considered: lower frequencies can always be used but they will insonify deeper tissue uselessly and will have a lower ratio of received to transmitted energy intensity.

Note also that equation 4.3 only considers the thickness of tissue between the artery and the skin and does not account for the attenuation in the blood. This agrees with the observation of Jensen (1996) that the attenuation of ultrasound in blood is smaller (about 0.2 dB/cm/MHz) than that in tissue (fat for instance has an average coefficient of 1.5 dB/cm/MHz).

#### **4.4 Mounting Angle**

The carotid artery is assumed to run parallel to the surface of the neck so that the mounting angle between the transducers and the skin sets the corresponding incidence angle. The assumption that the artery is straight is not exactly true anatomically but due to the fact that continuous monitoring is a relative rather than an absolute process, the error introduced by this assumption is secondary.

Equation 4.2 shows that the Doppler shift is related to the cosine of the incidence angle. Consequently, as this angle gets closer to zero the frequency shifts increase. The resulting spread in the frequency spectrum of the received signal leads to a more pronounced distinction between unfavorable low frequency components and the useful higher frequency components. In addition, the sensitivity of the measurement to uncertainties in the Doppler angle is the derivative of equation 4.2 by  $\theta$  and is given by

$$\left| \frac{\partial(\Delta F)}{\partial \theta} \right| = 2\nu \frac{f_o}{c} \sin \theta$$

Obviously, a smaller angle is desirable. However, decreasing the mounting angle  $\theta$  is subject to anatomical restrictions and it also results in an increase in the required depth of penetration of the ultrasonic beam. Typical clinical values for the probing angles for shallow vessels are in the range of  $30^\circ$  to  $60^\circ$  (Gill 1985) and we adopted an angle of  $45^\circ$  for the Doppler Necklace.

## 4.5 Location Uncertainty of the Artery

The ultrasound probes used in hospital diagnosis equipment are usually designed to emit a narrow beam that would focus the energy on the target vessel and increase the signal to noise ratio. The subject is typically at rest and the correct positioning of these probes is solely dependent on the skill of the human operator. The Doppler shift (which falls in the audible range) is played back through speakers and the operator moves the probe around until he/she hears the ‘highest pitched’ sounds in the signal. These sounds reflect the highest frequency components and indicate to the operator that the beam is intercepting the centerline of the artery.

The Doppler Necklace however, has to be used without human assistance and under circumstances when the location of the artery is uncertain or not fixed. This gives rise to a tracking problem. The uncertainty of the vessel location is in two dimensions: the transverse location as well as the depth. (If we adopt the coordinate system illustrated in figure 4.1, the transverse direction is the X-axis and depth is along the Z-axis). The latter uncertainty is handled by using CW beams that will pick up signals from all along their path. This depth insensitivity of CW beams could lead to intercepting flows in neighboring blood vessels in general. However, for the common carotid artery this problem does not arise: in the anatomical section shown in figure 2.1, it is evident that

there are no major arteries in the vicinity and any signal received will be representative of carotid flow only. Note however, that flow in the jugular vein might also be intercepted by the CW beam but can be differentiated from arterial flow because of its opposite direction and hence frequency shift. Also intercepting deeper arteries (like the vertebral artery) in the neck is unlikely because of the high reflection of ultrasound at the interface with the vertebral bone and because the high ultrasound frequency used in the Doppler Necklace will get significantly attenuated before reaching that depth.

The uncertainty in the transverse direction is resolved by designing an array of transducers that can provide coverage of a wide sector in the neck. Only the transducers that are favorably targeting the centerline of the artery are operated at any one time. Deciding on which transducers to operate is based on tracking the highest frequency shift (corresponding to the centerline velocity) in the signal. The inherent assumption is that the transducers have to be mounted close to the location of the artery initially. This can be achieved by using external features on the neck for guidance (such as pulse sensation) or by implementing a patient specific necklace.

The following sections will introduce the different possible approaches to solve the location uncertainty problem, the limitations of each and the reasons for selecting the array approach used.

#### **4.5.1 Using a Single Large Transducer**

The simplest approach to solve the tracking problem is to use a large ultrasound crystal. The beam generated by such a transducer will cover an area encompassing the artery and also allow for motion or location uncertainty. Matsumoto et al. (1989) carried out an experiment in which two semi-circular transducers of 1.5 cm diameter were used

to emit and receive the signal from the common carotid artery of an exercising subject. The transducers were mounted at 45° and were strapped around the neck of the subject (figure 4.2).

Such an approach is the most simple to implement but is not the most suitable configuration for continuous monitoring because of power consumption considerations: the emitter will be uselessly insonifying the regions around the artery. In addition, it is relatively bulky and lacks flexibility because the only parameter that can be varied is the amplitude of the voltage that drives the transducer.

### **4.5.2 Diverging Beam**

Another approach that we considered was to generate a beam that diverges off from the crystal and spans a sector in the neck. This approach is attractive because it would minimize the area covered on the skin. There are two basic methods to generate such a beam: either by using a flat transducer with a convex lens mounted in front of it, or using a transducer with a convex shape.

#### **4.5.2.1 Transducer with Convex Lens**

The main advantage of this configuration is the ready availability of flat transducers from several manufacturers. A lens would mount in front of the crystal and will have to cause divergence in the lateral X-direction while maintaining the same width of the beam in the Y direction. Both the material and the geometry of such a lens have to be specified.

Lenses for ultrasonic applications are usually manufactured from solids in which the velocity of sound is greater than that in water. Therefore diverging lenses are convex in shape. The relevant dimensions of a spherical lens are shown in figure 4.3. The focal

length  $F$  is the distance from the point on the curved surface on the central axis to the virtual point behind the lens where the extrapolated ‘rays’ emanating from the lens surface converge. For  $h < 0.1R$  (and consequently for small angles of incidence and refraction from the lens surface so that their sines are almost equal to their tangents), the relationship between the focal length and the radius is given by Wells (1979):

$$F = R/(1 - 1/n) \quad (4.5)$$

Where  $n$  is the refractive index of the material given by

$$n = c_1/c_2 \quad (4.6)$$

$c_1$  being the speed of sound in the lens and  $c_2$  that in the loading medium.

In addition to shaping the beam, the lens will also introduce phase aberration (for circular lenses), absorption losses and more importantly will create a reflection interface for the beam. Thus the ideal lens should be made of a material that has

1. a very high refractive index (to minimize the curvature)
2. zero attenuation
3. a characteristic impedance equal to that of the loading medium

Satisfying all these conditions is impossible because materials that usually have a high refractive index also have an impedance mismatch with water (and consequently with human tissue which is close to it). Polymethylmethacrylate and polystyrene are usually considered to offer the best compromise (Wells, 1979).

For the common carotid artery: assuming an average diameter of 7mm and a depth of 10mm: if we aim to cover a 14 mm wide region from a 5mm wide transducer

and taking into account the insonification angle of  $45^\circ$ , the resulting focal distance is 7.78 mm. For polysterene with a refractive index of 1.57 this yields a radius of curvature of

$$R = 7.78 \left( 1 - \frac{1}{1.57} \right) = 2.82 \text{ mm}$$

Which is an almost semi-cylindrical lens! Aluminum with a refractive index of 4.26 gives a more reasonable radius of curvature of about 6 mm. However, experimental evidence shows that an aluminum lens will create a high reflection interface and result in no detection of any useful signal.

#### **4.5.2.2 Using Curved Transducers**

Another alternative to produce a diverging beam is to have the crystal itself manufactured in a convex shape. The added complexity of producing the curved surface is offset by the fact that the issue of lens material is no more a problem.

#### **4.5.2.3 Limitations**

There is a main limitation when using a diverging beam generated by a single crystal whether with or without an acoustic lens: it is not a flexible design and as in the case of the configuration that uses a single large crystal, it could be uselessly insonifying regions in the neck that carry no signal.

A feature that is not an inhibiting factor for diverging beams but that should be mentioned nevertheless is the safe level of ultrasound energy to be used. When using a diverging beam and because of the need to maintain a certain level of energy at a particular depth, there results a concentration of acoustic energy at the face of the transducer. Assuming no attenuation for now, one can write out a simple relationship of energy conservation between the ultrasonic intensities  $I_1$  and  $I_2$  at two depths:

$$A_1 I_1 = A_2 I_2$$

Where  $A_1$  and  $A_2$  are the cross-sectional areas of the beam at the two depths. The ratio of the intensities is thus inversely proportional to the achieved divergence.

The FDA approved maximum ultrasound intensity for peripheral vessels is 310 W/cm<sup>2</sup>. A typical continuous wave probe (such as an Acuson 128XP) will produce about 0.4 W/cm<sup>2</sup>. This shows that energy concentration is not a serious drawback if a diverging lens was to be used.

### **4.5.3 Array Configuration**

From the sections above we can draw the conclusion that the most flexible way to provide coverage of a wide area in the neck is by using an array of small distributed transducers. These transducers can be selectively excited: one or more transducer at a time. In addition, a phase delay can be introduced between their input voltages when they are driven together.

#### **4.5.3.1 Mode of Operation: Phased Array vs Switching**

The phased array configuration is very common in both imaging and Doppler measurements using pulsed ultrasound. The basic concept is illustrated in figure 4.4: a time delay is introduced between the times at which each crystal is excited and the resulting wavefront can be steered in one direction or the other.

This idea can be extended to the case of continuous wave excitation of crystal. However, there is a limitation due to periodicity and the maximum possible time delay between any two transducers is limited to one period. For two transducers placed side by

side and activated with a delay between their voltages, the angle  $\phi$  at which a wavefront is steered away from its axial direction (figure 4.4) is given by

$$\phi < \sin^{-1}(\lambda/s) \quad (4.8)$$

where  $s$  is the spacing between the array elements and  $\lambda$  is the wavelength.

For an 8 MHz frequency, the wavelength  $\lambda=0.19\text{mm}$  and for a  $\phi$  as low as  $10^\circ$ , the spacing between the elements has to be smaller than 1mm.

Considering the added hardware complexity to implement variable time delays in exciting the crystals, it is obvious that adopting a phased array configuration does not offer an advantage over using multiple transducers that are excited in phase.

The proposed configuration for the Doppler Necklace is to have a multitude of crystals arranged so as to span a wide sector among themselves. At any one time, only the transducer or transducers that are favorably oriented and can potentially cover the centerline of the artery are switched on. Thus initially, the transducers are sequentially operated and the transducer with the highest velocity reading over one cardiac cycle is the one that is favorably targeting the centerline of the artery and is kept in emitting mode. If the patient is moving, variations in the location of the arterial centerline can be accounted for by activating more crystals around the optimally located one.

The parameters of the design are the dimensions of the crystals and the spacing between them. Furthermore, the transducers have to be operated as emitters or receivers and different considerations have to be accounted for.

## **4.5.3 Design of the Emitting Transducers**

The following sections present the factors that influence the determination of the dimensions of the emitting transducers and the spacing between them.

### **4.5.3.1 Vertical Dimension of Emitting Transducers**

The vertical dimension (along the Y-axis in figure 4.1) of the individual crystals to be used in the array is subject to two restrictions: the first is the velocity resolution achieved and the second is the need to have the carotid artery in the near field of the crystal.

#### **Velocity Resolution**

From sampling theory, it is known that limiting the observation time for any signal will limit the frequency accuracy that can be obtained.

If we consider a signal that consists of a single harmonic component and that is given by:

$$g(t)=\cos(2\pi f_0 t)$$

and if we observe this signal for an infinite period of time, its spectrum will be equal to two Dirac pulses: one at  $+f_0$  and the other at  $-f_0$ . However, infinite observation cannot be achieved practically and a limited observation time is equivalent to multiplying the signal by a window in the time domain. A rectangular window is given by

$$w(t)=1 \text{ when } 0 < t < T_{obs}$$

A multiplication in the time domain is equivalent to a convolution in the frequency domain. The Fourier transform of the rectangular window is a sinc function.

Convolving the sinc function with the two Dirac pulses of the original signal result in a broadening of the signal about  $+f_0$  and  $-f_0$ . As the window length increases, the width of the sinc function decreases and consequently there is less broadening of the original signal. In the limit when the window length is infinite, its Fourier transform is a Dirac function and no broadening of the original spectrum result. This phenomenon of spectral broadening takes place for all kinds of windowing functions, whether rectangular or of any arbitrary shape.

This concept can be extended to the case of the Doppler reading where the observation window is equivalent to the axial dimension of the insonified section and hence to the width of the ultrasonic beam when it intercepts the vessel. The limited observation window will smear the spectrum and result in frequency components that the original signal didn't have. The resolution limit set by spectral broadening cannot be improved by any later signal processing.

The relationship between the observation time  $T_{obs}$  and the desired spectral resolution  $B$  is given by

$$T_{obs} \cdot B \geq 1 \quad (4.9)$$

For the case of the Doppler Necklace, a continuous wave beam is intercepting the vessel at an angle of  $\theta$ . The observation time is equal to the time the blood cells are within the beam and is given by (Jensen 1996):

$$T_{obs} = D / (v \cdot \sin\theta) \quad (4.10)$$

Where  $v$  is the velocity of the blood cells and  $D$  is the dimension of the transducer. Note that the observation time depends on the velocity and even though there

are different velocities within the insonified region, the cells moving at slower speeds will get observed for a longer time. This keeps the relative frequency resolution constant and given by (Jensen 1996):

$$\frac{\Delta f_d}{f_d} = \frac{1}{T_{obs}} = \frac{\frac{v \cdot \sin \theta}{D}}{\frac{2v}{c} f_o \cos \theta} = \frac{c}{2Df_o} \tan \theta \quad (4.11)$$

For the Doppler Necklace: if we want to achieve a relative frequency resolution of 3% and taking the speed of sound in blood to be  $c=1560$ , using  $f_o = 8.1$  MHz and a mounting angle of  $45^\circ$  yields a dimension D of about 3.2 mm. Note however that this dimension will be equal to the height of the transducer only if the beam is collimated. This is explained further in the following section.

### Angle Uncertainty

Another factor to consider in setting the y-dimension of the crystal is the uncertainty in the reading that results from the variation in the intercept angle. In deriving the frequency resolution in the previous section, it was assumed that the angle  $\theta$  is constant. This would be true if the ultrasonic beam generated by the crystal was collimated and confined to a rectangular window at the location where it intersects the vessel. Actual continuous wave excitation beam patterns are complex (figure 6.1) and consist of a main lobe and a multitude of side lobes. Thus, exact assessment of the uncertainty in the frequency due to the spread in the intercept angle necessitates exact knowledge of the field. One commonly used approximation is to neglect the contribution of the side lobes and assume that all the energy is confined in the main lobe. The effective width of the beam would then equal the width of the main lobe. The main lobe

is not well defined for regions very close to the transducer face but further down into the near field it is equal in width to the corresponding dimension of the transducer up until the onset of the far field where it starts to diverge.

The depth at which the divergence starts is around the onset of the far field (Appendix A). For a circular transducer this depth is given by:

$$Z_R = D^2 / (4\lambda) \quad (4.12)$$

where  $D$  is the diameter and  $\lambda$  is the wavelength.

For rectangular transducers, there are no closed form solutions for  $Z_R$ . An approximation can be used based on the observation of Lockwood and Willette (that the near field inhomogeneity of a rectangular transducer is less marked than that of a circular one of similar size) and on the data measured by Stenzel (1952) and reproduced by Wells (1977). As a rough guide, the near field of a rectangular transducer extends to a distance somewhat beyond that of a circular transducer of diameter equal to the greater dimension of the rectangle.

For the Doppler Necklace, we want to estimate the vertical dimension of the transducers such that the resulting  $Z_R$  would be greater than the deepest location of the carotid artery. The slight overestimate of that dimension caused by using equation 4.12 can be considered a safety margin.

The relevant dimensions are the following:  $\lambda = 0.19$  mm and  $Z_R$  is about 17 mm (assuming an average diameter of 6.7mm for the carotid artery (Eriksen 1992) and a depth of 10 mm). The result is the need for a transducer with a height of 3.6 mm. As

discussed above, equation 4.12 provides a slight overestimate of the needed dimension but the resulting increase in near field depth can be regarded as a safety margin.

#### **4.5.3.2 Horizontal Dimension and Spacing of Emitting Transducers**

The horizontal dimension and spacing of the emitting transducers are related parameters. Among themselves, the transducers should be able to span a sector in the neck equal to the vessel diameter plus some allowance for location uncertainty. The total width spanned by the array was set as 14 mm for the Doppler Necklace. There are no hard rules in choosing the number of transducers: it is evident that the greater the number the more the complexity but the more the flexibility. However, a common restriction applies to all designs: the transducers cannot be spaced excessively apart or else there will be gaps in the overall ultrasound field due to the collimation of the individual beams.

For the Doppler Necklace, the number of transducers and their suggested spacing based on computer simulation is also discussed in section 6.2.4.

#### **4.5.4 Receiving Transducers**

The backscattering of ultrasound from red blood cells is discussed in Appendix A. The intensity of the backscattered signal is theoretically equal in all directions and experimental results published by Wells support this assumption. In that regard, there seems to be no constraints on selecting the location of the receiver. Since the emitting transducers will be selectively operated (and not all at once), any of the remaining idle transducers can be used as a receiver. However, upon further investigation, we found recommendations in literature to place the receiver and emitter close together so that they overlap in the distance. To understand this, we revisited the Doppler shift equation.

Equation 4.2 gives the Doppler shift for the case where the received beam is assumed to have retraced the path of the outgoing beam. For the Doppler Necklace, this is not necessarily true and it is better to generalize and define an angle  $\alpha$  between the emitted beam and the vessel and an angle  $\beta$  between the vessel and the receiving transducer. The Doppler shift equation is then rewritten as (Wells 1977):

$$\Delta F = \left( \frac{c - v \cos \alpha}{c + v \cos \beta} - 1 \right) f_o$$

and for  $c > v$

$$\Delta F = -\frac{f_o v}{c} (\cos \alpha + \cos \beta) \quad (4.13)$$

For the Doppler Necklace, the relationships between  $\alpha$ ,  $\beta$  and the spacing between the transducer elements can be derived from simple geometric relationships. Setting the maximum allowable error incurred in using the approximate form of the Doppler shift given in equation 4.2 at about 3% and if we consider the most shallow point occurring at 1 cm depth, this leads to a spacing of about 5mm. In other words, as long as the centerline of the receiver is within a distance of 5mm from that of the emitter, there is no need to account for the angle variation within 3% accuracy.

## 4.6 Transducer Selection and Mounting

The piezoelectric transducers used in the Doppler Necklace are to be operated in CW mode at a frequency of their resonant frequency ( $\sim 8$  MHz). Once the resonant frequency is specified, the piezoelectric crystals can be ordered from suppliers and are produced to have a thickness equal to an odd multiple of halfwavelengths.

In mounting the transducers, it is recommended to have the rear of the crystal air-backed i.e. uncovered (Jennings et al 1995). This is because upon excitation, two waves are generated at the center of the transducer and travel to both faces of the crystal. If one face is open to the air while the other loaded with some acoustic medium, complete reflection occurs at the interface with air (due to the acoustic mismatch) and the reflected wave will interfere constructively and reinforce the wave transmitted into the loading medium. The mounting of the crystals is schematically represented in figure 4.5.

## 4.7 Attachment to Skin

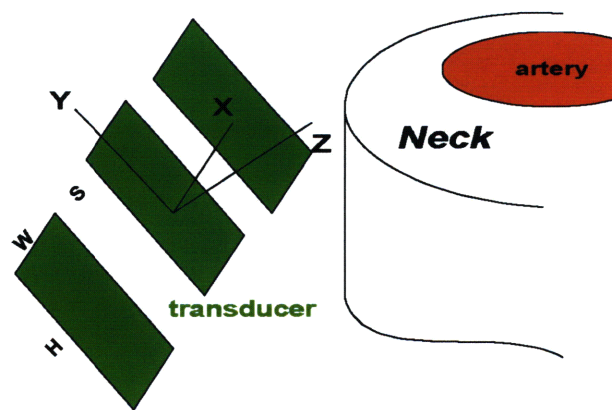
Ultrasound propagation from the transducer to the vessel and back necessitates the existence of a coupling medium other than air between the transducers and the skin. This is necessary because ultrasound will get reflected back from any interface that separates two mediums with different acoustic properties as in the case of air and tissue. In regular ultrasound diagnostic tests, it is common to use water-based gel to provide an acoustically nondissipative continuous medium between the patient's skin and the probe that the operator would be holding. For our application, the transducers have to be secured to the skin with an adhesive (fig 4.5) that would have a dual role of bonding and providing acoustic continuity. The adhesive should satisfy certain requirements, it should:

1. Adhere to the skin and cause no unacceptable irritation when used for extensive periods of time.
2. Easily removed without mechanically traumatizing the skin or leaving a residue upon removal.
3. Behave as an acoustically matching and nondissipative continuous medium.

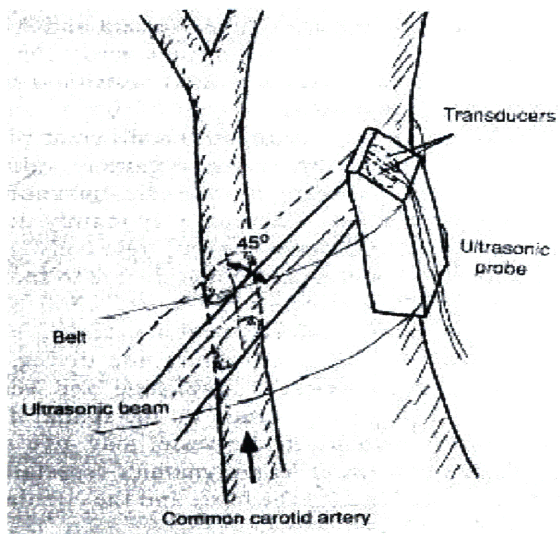
4. Provide a stiff bonding because if it is too compliant, the velocity due to the relative motion between the transducers and the skin (which is picked up by the Doppler) will become an unacceptable source of noise in the reading.

The first two criteria can be met with the existing technology in adhesives because they are not more stringent than the requirements on transdermal drug delivery adhesives. Current commercial transdermal drug delivery pads last up to 7 days (Venkatraman 1998). In addition, the load carrying requirement of the adhesive for our application is very low because the transducers are very small (0.23 x 2 x 5 mm each). Also, the transducers in the array are spaced to minimize skin coverage and they can be mounted at slightly different locations in order to relieve the skin between usages.

Meeting requirements 3 and 4 listed above is also possible with the current adhesive technology because ‘glues’ can be produced with different elastic moduli (Venkatraman 1998) and possibly with different acoustic properties.

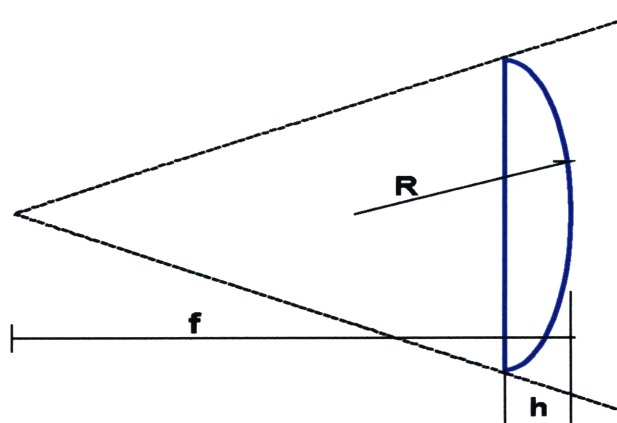


*Figure 4.1: Coordinates adopted to reference the transducers to the neck.*



*Figure 4.2: The setup used by Matsumoto et al (1989) to take continuous measurements at the common carotid artery consisted of two 15mm semicircular transducers.*

*Figure 4.3: parameters of the acoustic lens.*



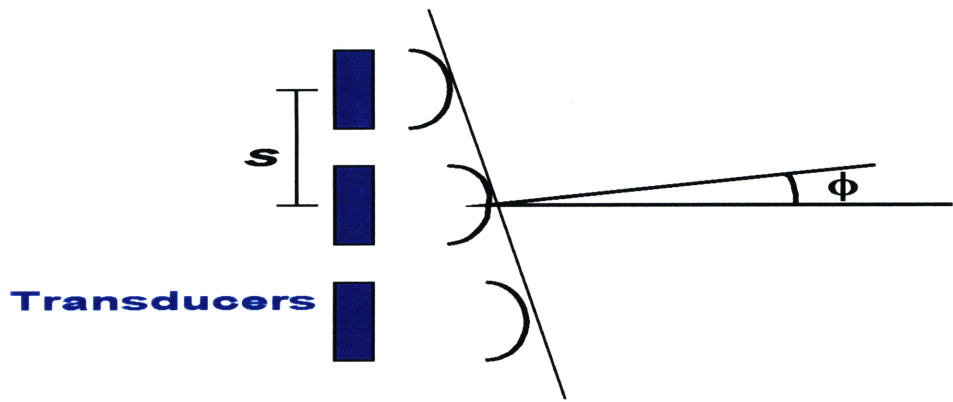


*Figure 4.4: driving the transducers with a delay creates a ‘steering’ effect by generating different wavefronts.*

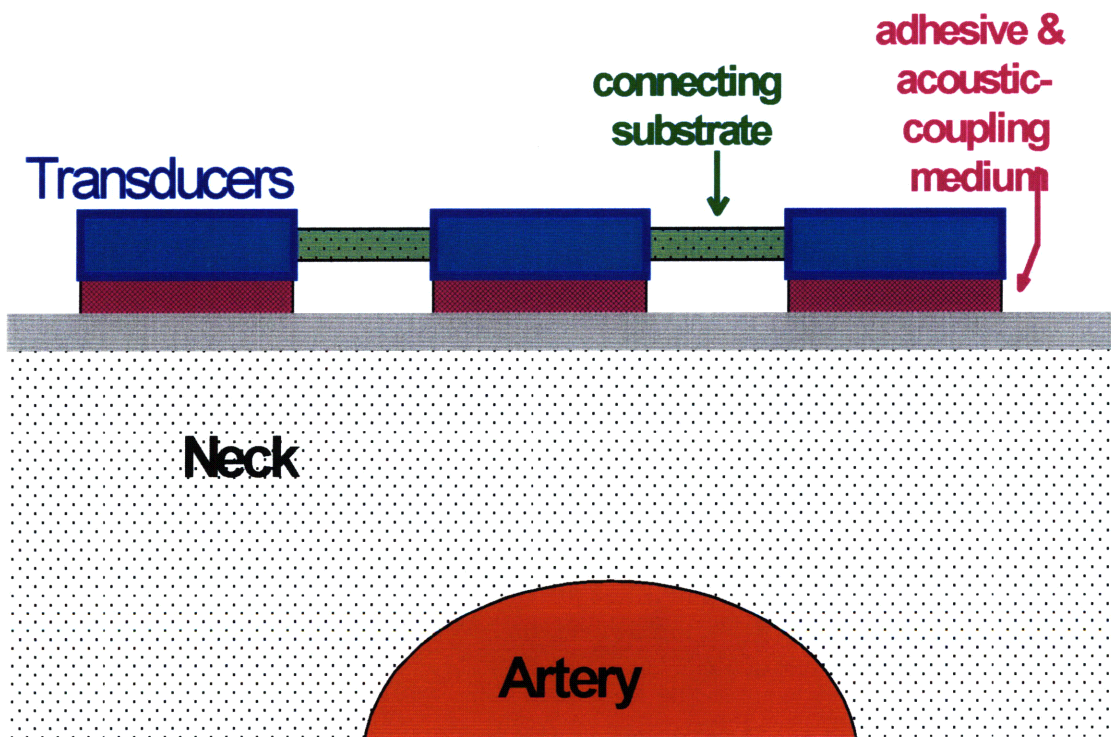


*Figure 4.5: Ideal mounting arrangement for the Doppler Necklace array: the individual crystals are air-backed and ‘glued’ to the skin with a proper acoustic coupling medium.*

## **Chapter 5**

### **Interpretation of the Signal**

The measurement taken by the Doppler sensor can be interpreted in different ways. Useful information can be derived from monitoring the fluctuations in the centerline velocity of the artery. In addition to that, the reading carries information on the velocity profile and can provide an estimate of flow. Also, the time rate of change of the pressure pulse can be recovered from the arterial wall motion.

#### **5.1 Monitoring Blood Velocity along the Centerline**

The blood velocity at the centerline of the artery can be easily monitored from the measurement taken by the Doppler Necklace. In the absence of both noise and intrinsic spectral broadening (ie infinite observation time – see section 4.5.3.2.1.1), the maximum frequency component  $F_{\max}$  present in the signal will exactly relate to the maximum velocity occurring in the vessel through the Doppler equation 4.2. The Doppler signal however, is not noise-free and the signal is not observed indefinitely. Thus, a proper algorithm is needed to estimate the maximum velocity within the accuracy allowed by the finite observation time.

Getting a physically meaningful value of  $F_{\max}$  necessitates that the ultrasound beam intercepts the region where the maximum velocity takes place. For a circular vessel, this region is at the centerline. Aside from this restriction, the value of  $F_{\max}$  estimated is not susceptible to beam intensity variations and the algorithm to find it is not complicated as shown in the following sections.

### **5.1.1 Finding $F_{max}$ as Energy Envelope**

One approach that is commonly used in diagnostic devices is to calculate  $F_{max}$  by finding the frequency component within which some specified percentage of the useful energy of the signal lies. The useful energy is the sum of the contributions of all frequencies above a certain threshold typically taken as 250Hz (Jensen). Frequencies below 250 Hz are due to reflections of the ultrasound at stationary or slowly moving tissue interfaces (such as vessel walls) and their very high amplitudes would render the algorithm useless.

### **5.1.2 Finding $F_{max}$ by Setting Threshold**

Another way to calculate  $F_{max}$  is by setting a threshold level for amplitude: any frequency component whose amplitude falls below the threshold is considered noise. In a typical hospital diagnostic test,  $F_{max}$  is superimposed on the sonogram and the operator can follow its evolution and make adjustments to the threshold level accordingly.

## **5.2 Estimating Flow and Velocity Profile**

The blood velocity  $V_{max}$  corresponding to  $F_{max}$  provides the primary criterion used by the Doppler Necklace to track the artery. It is also an important physiological parameter. However, because of fluctuations in arterial diameter and changes in the blood velocity profile over a cardiac cycle it cannot by itself provide an absolute assessment of blood flow. A better understanding of the flow in the artery can be achieved if its area weighted mean velocity can be estimated.

The Doppler signal carries information in both its frequency and amplitude. There are several approaches to recover information about the flow distribution but they all rely on the following idea:

The received Doppler shift consists of different frequency components (corresponding to the different velocities in the vessel) occurring with different amplitudes. Assuming that the angle of incidence onto the blood vessel is fixed and that the beam is illuminating the target volume uniformly, the amplitude of each Doppler frequency component will be proportional to the number of cells moving at the respective velocity. Thus the frequency spectrum which is a plot of amplitude versus frequency can be thought of as a plot of cell count versus velocity (Nanda 1985). In addition, if the spatial concentration of cells is uniform within the vessel, the Doppler spectrum can be thought of as flow area (instead of cell count) versus velocities. Figure 8 illustrates this idea and shows the spatial maximum and mean velocities as well. Section 5.1 discussed how the spatial peak velocity (at the centerline) can be recovered from the signal. The spatial mean velocity is given by:

$$V_{mean} = \frac{\int v.dA}{\int dA} \quad (5.1)$$

Assuming uniform insonification of the vessel, the spatial mean velocity is directly related via the Doppler equation to the mean frequency in the signal given by:

$$F_{mean} = \frac{\int_0^\infty fP(f).df}{\int_0^\infty P(f).df}$$

### 5.2.1 Zero-Cross

One method to determine the dominant frequency component in the signal is to use a zero-crossing detector. This algorithm counts the number of times the signal crosses its mean value and can be easily implemented electronically. The number of zero crossings per second is given by:

$$N_z = 2 \sqrt{\frac{\int_0^{\infty} f^2 P(f) df}{\int_0^{\infty} P(f) df}} \quad (5.3)$$

where  $f$  and  $P(f)$  are the frequencies in the signal and their corresponding magnitudes. This equation shows that the output of the zero-cross detector is twice the RMS frequency of the signal. The RMS value is higher than the spatial mean frequency given by equation 5.2 and the ratio of  $N_z$  to  $F_{mean}$  depends on the velocity profile index that changes over the course of the cardiac cycle. Due to this limitation, the output of the zero cross detector only provides a crude estimate of mean velocity and cannot be used to estimate blood flow even under conditions of uniform insonification. In addition, it is vulnerable to both high and low frequency noise. Better insight on the frequency distribution in the vessel is possible by sampling the signal and manipulating its Fourier transform.

## **5.2.2 Spectral Analysis of the signal**

### **5.2.2.1 First moment of Area**

Looking back at equation 5.2 for  $F_{mean}$ , we notice that the numerator relates to the numerator in equation 5.1 for  $V_{mean}$ . Since the latter is equal to the total blood flow in the artery, one can conclude that the first moment of area of the spectral distribution of the Doppler signal about the zero frequency axis gives a dimensionless estimate of blood flow volume without knowledge of the vessel diameter. In an actual measurement discrete Fourier transforms are used and the integral is replaced with a finite summation over the individual frequencies.

The main limitation of this approach is that even under ideal conditions, the correlation factor between the first moment of area of the Doppler spectrum and the flow depends on the varying spatial concentration of blood cells i.e. the hematocrit (see Appendix B).

### **5.2.2.2 Mean Velocity and Flow Profile**

Another possible approach to measure the flow is by estimating the mean velocity from the Doppler signal and by measuring a priori the diameter of the vessel averaged over a cardiac cycle with ultrasound imaging. Eriksen (1992) has shown that the error incurred in calculating the flow volume by using the average diameter of the vessel instead of the real time diameter is less than 3% for the common carotid artery.

The mean velocity is related to both the maximum velocity and the flow profile. Starting from the velocity distribution for a circular artery:

$$V(r) = V_o[1 - (r/R)^p]$$

The relationship between  $V_o$ ,  $V_{mean}$ , and  $p$  is then:

$$V_{mean} = \frac{\int_A v.dA}{\int_A dA} = \frac{\int_0^R V_o(1-(r/R)^p) \cdot 2\pi r dr}{\pi R^2} = 2V_o \left(\frac{1}{2} - \frac{1}{p+2}\right)$$

upon rearranging, this yields

$$p = 2V_{mean}/(V_o - V_{mean}) \quad (5.5)$$

and relating that to the frequencies:

$$p = 2F_{mean}/(F_{max} - F_{mean}) \quad (5.6)$$

### 5.2.3 Effect of Acoustic Distribution

The equations presented above assume that the ultrasound field is uniform over the insonified area. This assumption is not exactly true and the following sections discuss beam formation and uniformity.

#### 5.2.3.1 Beam Formation

*Note: The propagation medium is assumed lossless (i.e. without attenuation) for the following derivation but this assumption is revisited later.*

Huygen's principle states that the radiation pattern from a source of arbitrary shape can be found by modeling the source as a collection of point sources each radiating spherical waves. The summation in magnitude and phase of the contribution of all point sources forms the resulting field. Thus the incremental pressure contribution  $dp$  from each point on the transducer face at the observation point is given by (Christensen 1988):

$$dp = (kZu_o/2\pi r') \cos(\omega t - kr' + \pi/2) ds \quad (5.7)$$

where:

$$k = 2\pi/\lambda \quad (\lambda \text{ is the wavelength})$$

$Z$  = acoustic impedance of the medium

$u_o$  = the amplitude of the velocity in the z-direction at which the source surface is vibrating:  $u = u_o \cos(\omega t)$ . For small size transducers as in the case of the Doppler Necklace all points on the surface can be safely assumed to be oscillating with the same velocity and in phase with one another.

$r'$  = distance from the contributing point on the transducer surface to the observation point (see fig 5.2).

Thus the total pressure at the observation point is given by:

$$p = \int_{source} dp \quad (5.8)$$

For the case of rectangular transducers like the ones employed in the Doppler Necklace, there is no closed form solution to find  $p$  and numerical simulation of the field has to be performed. However, a common feature of pressure fields of transducers of all shapes is the existence of a near field and a far field.

In the near field the magnitude of  $p$  is characterized by rapid oscillations and considerable constructive and destructive interference while in the far field it drops at a rate of  $1/z$ . For a circular transducer of diameter  $D$ , the transition from near to far field along the axis of the transducer takes place at a distance of  $D^2/4\lambda$  (figure 5.3).

The power intensity of the ultrasonic field is defined as:

$$I = p^2/Z$$

Another parameter relevant to ultrasonic insonification is the angle at which the beam diverges: a plot of the power density pattern versus distance away from the face of

a circular transducer reveals the existence of one main and several side lobes. The majority of the power being contained in the main lobe, the effective width of the beam is commonly taken to be equal to the width of the main lobe at any particular depth. The beam remains collimated in the near field but diverges in the far field with an angle  $\theta$  given by:

$$\theta = \sin^{-1}(\lambda/h)$$

where  $h$  for a rectangular transducer is the corresponding dimension in the plane of  $\theta$  (Christensen 1988).

Note on attenuation: The effect of attenuation has not been included in the equations above and it was not included in the computer simulations performed. The reason is that although the attenuation in tissue limits the depth from which a useful signal can be obtained, attenuation in blood is low (with a value of about 0.2 dB/cm/MHz compared to a value of 1.5 dB/cm/MHz in fat) and Jensen (1996) reports that ‘the signal received from the part of the vessel that is furthest away from the transducer is not much more attenuated than that close to the transducer’.

### 5.2.3.2 Beam Uniformity

Achieving perfect beam uniformity over a wide area is impossible practically or even theoretically. In order to decrease nonuniformity of the acoustic field by decreasing the intensity of sidelobes, it is common to use a transducer with the shape of a split annular array and to drive the outer ring with less voltage than the inner ring. Wells reports that even a transducer consisting of two annular rings can give satisfactory results. Evans et al (1989) have used a pulsed wave configuration with proper phasing to generate

a wide beam that is almost uniform at a certain depth. In all cases, hardware complexity is increased.

For the Doppler Necklace, the approach was to try to achieve some field uniformity by varying the size and spacing of individual transducers in the array configuration.

### **Operating around the onset of the far field**

In this approach, the attempt is to operate around the onset of the far field. In that region, the field is not irregular like in the near field and has not dropped considerably yet. However, the depth at which the artery lies is not known and computer simulations have shown that when two transducers are placed next to one another, they fail to cover the region in between them uniformly.

### **‘Speckle effect’**

We also investigated a novel idea by attempting to increase the spatial rate of nonuniformity to achieve a fine ‘speckled’ field. The concept stems from the fact that velocity is a function of radial distance in the artery and if the discontinuities in the ultrasound field are closely spaced, they have a circumferential averaging effect that reduces the error. Computer simulations were performed and the results looked promising: properly spaced small transducers would generate close nonuniformities in the acoustic field. However, upon further investigation, this idea turned out to be of little use for the Doppler Necklace due to the following reason:

The size of the transducers influences the spacing of the variations in the field and the depth to which the close variations persist. As the first parameter decreases the second decreases but the third rises. Thus small crystals generate fine uniformities but over a

shallow depth, while bigger transducers generated coarse non-uniformities over a deeper region. Section 6.2.3 shows the results of the simulations carried out.

### 5.2.3.3 Accounting for Beam Nonuniformity

Instead of assuming uniformity of the beam, it is obviously more accurate to account for the acoustic field distribution nonuniformity. However, this would necessitate knowledge of the in-vivo distribution of the field. We had a different approach in trying to reconstruct the field from the measurement itself: by assuming parabolic flow during diastole, the distorting effect of the acoustic field can be recovered as a function of the radius. A polynomial is then fitted to approximate the field and is used during systole and the rest of the cardiac cycle. The formal derivation of this concept is as follows:

Starting with the typical velocity distribution in a cylindrical vessel described by the equation:

$$v(r) = V_o \left( 1 - \left( \frac{r}{R} \right)^p \right)$$

The frequency shifts  $f_d$  are derived from the Doppler equation:

$$f_d(r) = 2V \frac{f_o}{c} \left( 1 - \left( \frac{r}{R} \right)^p \right) \cos \theta \quad (5.9)$$

where the incidence angle  $\theta$  has been assumed to be  $45^\circ$  for the carotid artery.

The amplitude of the signal at the corresponding frequencies is found by first calculating the number of contributors (or scattering particles) moving with a velocity  $v < v_I$

$$n_p(v < v_I) = \int_{r_I}^R l 2\pi r \rho_p dr = l \pi \rho_p (R^2 - r_I^2) \quad (5.10)$$

where  $\rho_p$  is the spatial concentration of blood cells. In discrete form, this is given by:

$$n_p(v < v_1) = \sum_{r_i=r_1}^R l 2\pi r_i \Delta r \rho_p \quad (5.11)$$

We now lump the effect of the acoustic distribution so that its effect can be represented as a sole function of radius  $G(r_i)$ . The resulting power density spectrum is given by

$$P_v(v) = G(r_i) \frac{\Delta n_p}{\Delta v} = G(r_i) \frac{\sum_{r_i=r_1+\Delta r}^R 2\pi r_i \Delta r \rho_p - \sum_{r_i=r_1}^R 2\pi r_i \Delta r \rho_p}{\Delta v} = G(r_i) \frac{-2\pi r_i \Delta r \rho_p}{\Delta v} \quad (5.12)$$

but,

$$\Delta r = R(1 - \frac{v_i}{V_o})^{\frac{1}{p}} - R(1 - \frac{v_i - \Delta v}{V_o})^{\frac{1}{p}} \quad \text{and by simple manipulation gives:}$$

$$\begin{aligned} \Delta r &= R \left[ \left( 1 - \frac{v_i}{V_o} \right)^{\frac{1}{p}} - \left( 1 - \frac{v_i}{V_o} + \frac{\Delta v}{V_o} \right)^{\frac{1}{p}} \right] = R \left[ \left( 1 - \frac{v_i}{V_o} \right)^{\frac{1}{p}} - \left( 1 - \frac{v_i}{V_o} \right)^{\frac{1}{p}} \left( 1 + \frac{\Delta v / V_o}{(1 - v_i / V_o)} \right)^{\frac{1}{p}} \right] \\ &= R \left[ \left( 1 - \frac{v_i}{V_o} \right)^{\frac{1}{p}} \left\{ 1 - \left( 1 + \frac{\Delta v / V_o}{p(1 - v_i / V_o)} \right) \right\} \right] = R \left( 1 - \frac{v_i}{V_o} \right)^{\frac{1}{p}} \left\{ - \frac{\Delta v / V_o}{p(1 - v_i / V_o)} \right\} \end{aligned}$$

so that:

$$\frac{\Delta r}{\Delta v} = \frac{R}{p} \left( 1 - \frac{v_i}{V_o} \right)^{\frac{1}{p}} \frac{1/V_o}{1 - v_i / V_o} = -\frac{R}{pV_o} \left( 1 - \frac{v_i}{V_o} \right)^{\frac{1}{p}-1} \quad (5.13)$$

substituting back into equation 5.12 yields:

$$P_v(v) = G(r_i) \frac{l 2\pi r_i \rho_p R}{pV_o} \left( 1 - \frac{v_i}{V_o} \right)^{\frac{1}{p}-1}$$

$$\text{but } r_i = R(1 - v_i / V_o)^{\frac{1}{p}}$$

and the final form of the spectral power distribution is then:

$$P_v(v) = G(r_i) \frac{l 2\pi \rho_p R^2}{pV_o} \left( 1 - \frac{v_i}{V_o} \right)^{\frac{2}{p}-1} \quad (5.14)$$

The constant terms of equation 5.14 (assuming  $R$  to be fixed) can be lumped together into one term  $K$ , and  $P_v(v)$  is then expressed as

$$P_v(v) = G(r_i) \frac{K}{pV_o} \left( 1 - \frac{v_i}{v_o} \right)^{\frac{2}{p}-1} \quad (5.15)$$

Theoretically, the spectral distribution  $P_v(v)$  can be recovered from the measured Doppler shift. Knowledge of the value of  $p$  will lead to knowledge of the acoustic field distribution and vice versa.

Several researchers (Wang et al. 1995, Brands et al 1995) report that flow during diastole in the common carotid artery phase is parabolic. Assuming a  $p=2$  during diastole, and since  $P_v(v)$  is a measured and  $V_o$  can be recovered, the acoustic distribution  $G(r_i)$  can be derived. This information can then be applied to other phases of the cardiac cycle to recover the remaining velocity profiles.

Computer simulations of this algorithm are reported in section 6.4. This algorithm offers a very strong advantage in that the beam need not cover the whole carotid artery: the inequality in coverage will be accounted for. Actual experimental measurements that were processed using this algorithm are reported in chapter 6 together with the reason for the deviation of the measurements from the theoretical analysis.

### 5.3 Wall Motion

In addition to carrying information on blood velocity, the Doppler sensor also picks up the vessel wall motion. This signal is usually of low frequency (<250Hz) but of high amplitude: 10 to 100 times greater than the amplitudes of blood velocity shifts (Jensen 1996). It is common practice in medical diagnosis to filter out. However, as the

following section shows, the wall velocity is related to the time rate of change of the pressure waveform.

Assuming the artery to be of circular cross-section: the fluid flow in the tube is incompressible so that the equation of continuity is given in cylindrical coordinates by

$$\frac{\partial u}{\partial x} + \frac{1}{r} \frac{\partial}{\partial r} (rv) + \frac{1}{r} \frac{\partial w}{\partial \theta} = 0 \quad (5.16)$$

where  $u$  is the longitudinal component of the velocity and  $v$  is the radial component and  $w$  is the circumferential component. Assuming the flow in the carotid artery to be axisymmetric so that  $w=0$  and  $(\delta/\delta\theta)=0$ , this simplifies the continuity equation 5.16 to the following form

$$\frac{\partial u}{\partial x} + \frac{1}{r} \frac{\partial}{\partial r} (rv) = 0 \quad (5.17)$$

Considering a segment of the carotid artery as an elastic segment of a tube of radius  $a$  which undergoes vibrations in the transverse direction only. The instantaneous radius of the tube is given by  $a+\eta(x,t)$  where the vibrations are very small relative to the initial radius namely  $\eta \ll a$ . Eriksen (1992) reports the average percentage variation of the diameter of the carotid artery from its mean as 6.7% so the assumption we just made is not perfectly satisfied, but is valid for a first order approximation.

The average axial velocity is found by integrating the velocity across the tube cross section, since we assumed small vibration, it is given by:

$$\bar{u}(x,t) = \frac{1}{\pi a^2} \int_0^a u(x,r,t) \cdot 2\pi r dr \quad (5.18)$$

Integrating the equation of continuity (5.17) across the tube and inserting equation (5.18) results in the following relationship:

$$\pi a^2 \frac{\partial \bar{u}}{\partial x} + 2\pi r v(x, r, t) \Big|_{r=0}^{r=a} = 0 \quad (5.19)$$

The radial velocity at  $r=0$  vanishes because of symmetry and the the radial velocity at  $r=a$  is the wall velocity and will be denoted by  $v_w(x, t)$ , it follows that

$$v_w(x, t) = -\frac{a}{2} \frac{\partial \bar{u}(x, t)}{\partial x} \quad (5.20)$$

Assuming the flow to be non-viscous (ie viscous effects are small over the section being observed) the equations of motion will be given by:

$$\rho \left( \frac{\partial u}{\partial t} + u \frac{\partial u}{\partial x} + v \frac{\partial u}{\partial r} \right) = -\frac{\partial p}{\partial x} \quad (5.21)$$

$$\rho \left( \frac{\partial}{\partial t} + u \frac{\partial u}{\partial x} + v \frac{\partial v}{\partial r} \right) = -\frac{\partial p}{\partial x} \quad (5.22)$$

The approximation of neglecting the viscous terms implies that the wave travels without attenuation, this is definitely wrong for the arterial system as a whole but can be used over a small section of the carotid artery.

Further simplification of the equations above can be performed with dimensional analysis. If the speed of propagation of the wave is  $c$ , its frequency is  $f$  and its wavelength is

$$\lambda = c/f$$

We can use  $\lambda$  and  $1/f$  as characteristic length and time respectively. The average velocity  $\bar{u}$  is used as the characteristic velocity. The ratio of the inertial terms to the acceleration in the equation above become:

$$\frac{u \frac{\partial u}{\partial x}}{\frac{\partial u}{\partial t}} \sim \frac{\bar{u} \cdot \frac{\bar{u}}{\lambda}}{\frac{\bar{u}}{1/f}} = \frac{\bar{u}}{f \cdot \lambda} = \frac{\bar{u}}{c} \quad (5.23-a)$$

$$\frac{u \frac{\partial v}{\partial x}}{\frac{\partial v}{\partial t} - \frac{v^*}{1/f}} \sim \frac{\bar{u} \cdot \frac{v^*}{\lambda}}{\frac{v^*}{c}} = \frac{\bar{u}}{c} \quad (5.23-b)$$

we can safely assume that

$$\frac{\bar{u}}{c} \ll 1$$

since the maximum possible value of this term is  $.4/5=0.08$  (occurring at the aorta) and the average value in the cardiovascular system is 0.01. Equation 5.23 also contained  $v^*$  which is the characteristic radial velocity and can be equated to the radial wall velocity:

$$v^* = v_w = -\frac{a}{2} \frac{\partial \bar{u}}{\partial x} \sim \frac{-a\bar{u}}{2\lambda} \quad (5.24)$$

performing the dimensional analysis for  $v$  gives:

$$\frac{v \frac{\partial u}{\partial r}}{\frac{\partial u}{\partial t} - \frac{v^*}{1/f}} \sim \frac{\frac{v^*}{a} \frac{\bar{u}}{c}}{\frac{\bar{u}}{c}} \sim -\frac{\bar{u}}{c} \ll 1$$

$$\frac{v \frac{\partial u}{\partial r}}{\frac{\partial u}{\partial t} - \frac{v^*}{1/f}} \sim \frac{\frac{v^*}{a} \frac{v^*}{c}}{\frac{v^*}{c}} \sim \frac{\bar{u}}{c} \ll 1$$

Thus the inertial terms can be assumed to be small compared to the instantaneous acceleration and the resulting equations are:

$$\rho \left( \frac{\partial u}{\partial t} \right) = - \frac{\partial p}{\partial x} \quad (5.25)$$

$$\rho \left( \frac{\partial v}{\partial t} \right) = - \frac{\partial p}{\partial r} \quad (5.26)$$

Furthermore, comparing the relative magnitude of:

$$\frac{\partial p / \partial r}{\partial p / \partial x} \sim \frac{a}{\lambda}$$

we conclude that since the speed of propagation is very high and the frequency is low (heart beat frequency is about 1 Hz) the corresponding wavelength is large and consequently much greater than the tube radius. Therefore, it can be assumed that pressure is a function of axial distance only and if equation 5.25 is integrated over the vessel diameter, it follows that (Dinnar 1983):

$$\rho \frac{\partial \bar{u}}{\partial t} = - \frac{\partial p}{\partial x} \quad (5.27)$$

Now let us analyze the stress in the vessel wall: assuming that the wall has a linear relationship between stress and strain and is incompressible so that its Poisson's ratio is 0.5, we have:

$$\sigma = E \cdot \varepsilon$$

and

$$\varepsilon = \eta / a$$

The circumferencial tension T is the result of multiplying the stress per unit length by the thickness of the tube h:

$$T = \sigma \cdot h = E \cdot \varepsilon \cdot h = E \cdot h \cdot \frac{\eta(x,t)}{a}$$

Considering that this tension is balanced by the inner pressure and wall inertia, and for an elemental segment we get:

$$\frac{Eh\theta}{a} \eta = a\theta \cdot p - \rho_w (a\theta h) \ddot{\eta}$$

where the angle is considered small for the elemental segment so that  $\sin\theta \sim \theta$ .

Rearranging the terms, we get pressure as a function of wall motion as:

$$p = \frac{Eh}{a^2} \eta + \rho_w h \ddot{\eta} \quad (5.28)$$

at the wall interface, the solid wall and the fluid velocities must match so that no separation results and this gives the following equality (Dinnar 1983):

$$v_w(x, t) = \dot{\eta}(x, t)$$

Assuming the vessel wall to be thin (as in the case of the carotid artery), we can then neglect the second inertia term of equation 5.28. Taking the derivative of p and substituting in equation 5.20 gives the final relation:

$$\frac{dp}{dt} = \frac{Eh}{a^2} \cdot v_w(x, t) \quad (5.29)$$

This relates the vessel wall motion to the time rate of change of the pressure pulse traveling through the arterial section under consideration.

#### **5.4 Carotid Flow as Index of Diastolic Cerebral Flow**

As mentioned earlier, Matsumoto et al. (1992) had used the common carotid artery flow as an index of cerebral flow. Champagne and Farget (1980) support this idea by the fact that circulation to the brain is normally of low resistance and diastolic flow in the internal carotid artery is relatively large. On the other hand, the area supplied by the external carotid artery has a high-resistance bed so that diastolic flow is a small fraction of the total flow and is sometimes even absent. Thus the diastolic flow in the common carotid artery almost entirely ends up as internal carotid flow to supply the brain.

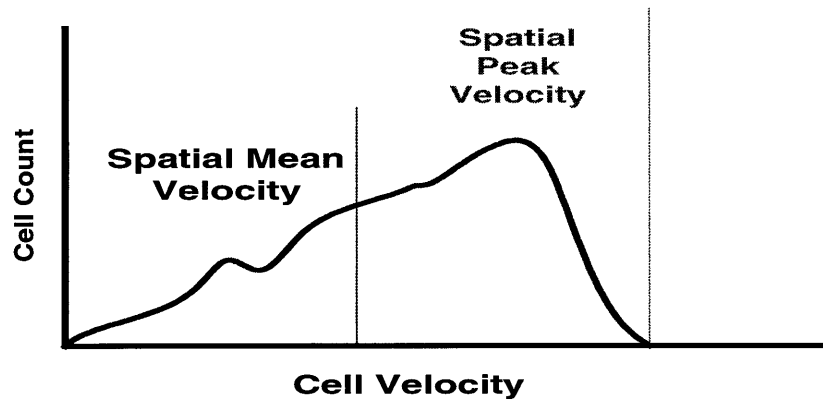


*Figure 5.1: Doppler frequency spectrum shown as cell count vs cell velocity plot.*

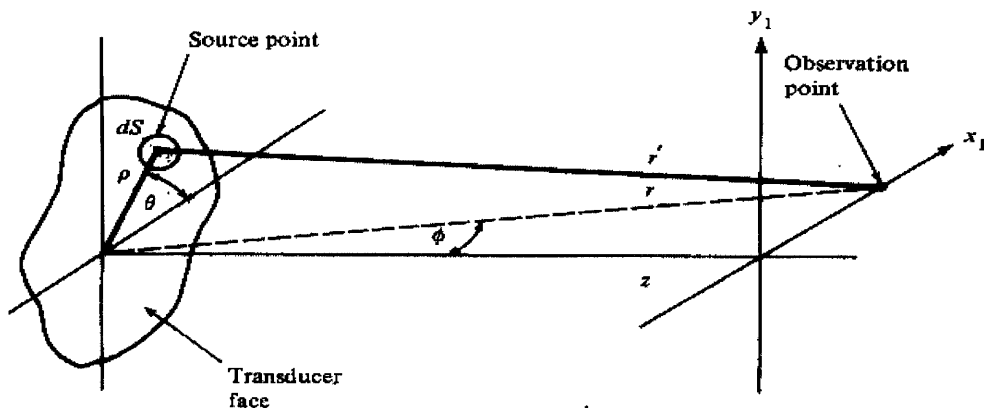


*Figure 5.2: Reference frame used in calculating the acoustic field distribution(Christensen 1988).*

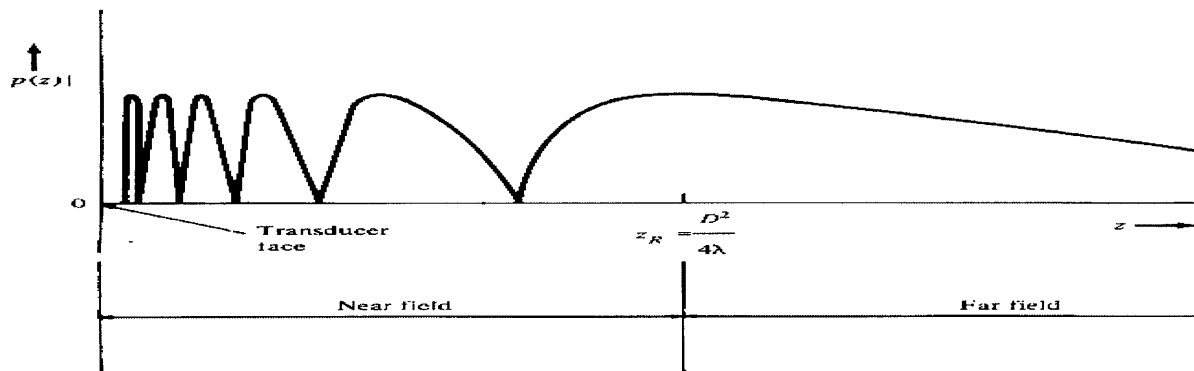


*Figure 5.3: variation of the magnitude of the on-axis pressure field from a circular transducer (Christensen 1988).*

# Chapter 6

## Experimental Results and Computer Simulations

### 6.1 Overall Setup

The electronics used in the Doppler Necklace is an adaptation of the commercial unit Model 909 Directional Doppler produced by Parks Medical Electronics. The original unit has dual frequency operation of 4 MHz for deep vessels and 8.1 MHz for shallow ones. The unit generates a sinusoidal driving voltage to the transducers and recovers the Doppler shift from the received signal by multiplying the outgoing signal with the ingoing one in a process known as ‘mixing’. The device then performs directional filtering of the Doppler signal and separates the signal caused by flow towards the transducer from that caused by flow away from it. The device also outputs a zero-cross detector trace.

In all the experiments the 8.1 MHz mode was used. The broadband unprocessed signal was tapped out of the device and digitally sampled at 20 kHz into a *Labview 5.0* environment. *Matlab* was used to perform signal processing as well as to do computer simulations. The standard toolboxes and the special toolbox *Ultrasim 2.1* © (written by Sverre Holm et al for ultrasound field simulation) were used.

### 6.2 Simulating the Ultrasonic Field Distribution

The individual transducers used in all experiments were rectangular in shape: 2mm by 5mm and were identical to the ones used in the original probes of the Parks device.

### **6.2.1 Field for an Individual Crystal**

The following convention was used in naming the axes (figure 4.1) with the origin (0,0,0) being at the center of the transducer:

1. The x-axis is along the aperture of the transducer.
2. The y-axis is along the height of the transducer.
3. The z-axis is the depth direction (into the neck)

Figure 6.1 shows the distribution at  $y=0$  of the magnitude of the intensity of the ultrasonic field for the 2mm by 5mm crystal used. The x direction of the transducer is the vertical axis in the plot and depth is the horizontal axis. The near field and the side lobes are apparent in the plot. The carotid artery would normally lie at a depth of about 10 mm. Since the transducer is mounted at  $45^\circ$ , the corresponding region of interest in the plot is around a depth 15 mm. In that region, the energy emitted by the transducer is still mostly contained within a 2mm band (same as the x dimension of the transducer).

### **6.2.2 Field Generated by a Convex Tranducer**

We mentioned in section 4.5.2.2 that one method to generate a wide diverging beam was to use a convex transducer. Such a configuration would distribute the acoustic energy over a wider sector but fails to create a homogeneous field. Figures 6.2 and 6.3 compare the simulated intensity fields of a planar and a convex crystal (x-dimension is 5mm and the radius of curvature is 20 mm). It is apparent that the main and side lobes of the field of the planar transducer seem to have split up into smaller lobes.

### **6.2.3 Field Uniformity**

Previous investigators have achieved beam uniformity at the expense of complexity in electronics by using annular arrays of independently driven discrete

transducers (Christensen 1988). Although perfect uniformity is theoretically impossible to achieve, one way to alleviate the problem is to have the artery fall in the region just before the onset of the far field. In that region the field varies slowly over distance. Another novel way approach that we investigated was to make the maxima and minima closely spaced in the region of interest. Numerical simulation shows that such a field with closely spaced peaks has an ‘averaging’ effect and tends to decrease the error in the flow estimate. Figure 6.4 illustrates the concept where the variations in the field are occurring over small spatial distances. Further investigation showed that for small transducers, the distance up to which this ‘speckling’ effect persists is not deep enough to be of practical usefulness for the Doppler Necklace. Bigger transducers were used in an attempt to drive the speckling effect further but they failed to provide the fine speckling needed. Figures 6.4 and 6.5 show the effect of increasing the size of the transducers.

#### **6.2.4 Multiple Emitters**

Based on results from several simulations we recommended an arrangement of 5 Parks crystals with 1mm spacing between them. The computer simulation was carried out and the resulting field is shown in figure 6.6. Among themselves, the transducers can provide coverage for a sector of about 14 mm wide.

An experimental setup was used to check the validity of the concept of using multiple transducers driven in phase to cover a wider area. The setup is shown in figure 6.7: water is circulated through a narrow slit of 1mm width. The first experiment was to check the effect of receiver location on the signal: the emitter location was fixed and the receiver was moved along the y direction using a micrometer table. The results showed that the backscattering could not be assumed to be uniform in all directions but it

preferentially favored the vertical direction. This could be due to the fact that the fluid flow is confined to a narrow space and so backscattering through the sides would get attenuated because of reflection at the channel walls.

In order to eliminate the effect of receiver location variations, the receiver was fixed and the emitter was moved along the Y-axis using a micrometer table. The measured data resulting from using two crystals as emitters (with 1 mm spacing between them) was compared to that resulting from the use of only one emitter. The result is shown in figure 6.8: a plot of the voltage output from the zero-cross detector of the Parks device is shown versus lateral displacement of the emitter. Since the flow and hence the flow profile is constant, the zero-cross output would relate to the RMS frequency in the signal (see section 5.2.1). It is evident from figure 6.8 that two spaced transducers used as emitters can provide coverage of a wider area than the sum of their individual widths. This was shown in the computer simulation and is due to the superposition of side lobes.

### **6.2.5 Multiple Receivers**

Experiments were also performed to test the usefulness of having multiple receivers. The emitter and receiver positions were fixed and the output from using one receiver crystal was compared to that from using two crystals. There was no advantage in using multiple receivers: the received signal was not improved and in some cases deteriorated. The deterioration was possibly because the receiving transducers were connected in parallel. Due to the difference in traveling time of the backscattered signal to each of the transducers, simple parallel connection could lead to non-constructive summation. The added complexity of implementing an array-receiving algorithm to

account for the phase lag between multiple receivers and recover directional information is not justified: a single receiver provides satisfactory results.

### 6.3 Tracking the Centerline Velocity

One mode of operation of the Doppler Necklace array is to have only one transducer emitting at any one time and another receiving. The emitter, being of small aperture, creates a narrow beam that should intercept the centerline of the artery. The latter condition is met by alternately exciting the different transducers and selecting the one that gives the maximum velocity reading over a cardiac cycle. To illustrate this concept, data was taken when only one transducer was emitting and providing the highest possible frequency. The Doppler measurement was sampled at 20 KHz. The signal was then high-pass filtered to get rid of all components less than 200Hz. These low frequency components are of high amplitude and correspond to vessel wall activity as well as relative motion between the crystals and the skin. This process of high pass filtering sets the lowest detectable velocity value at about 2.7 cm/sec (corresponding to 200 Hz). Figure 6.9 shows  $F_{max}$  corresponding to an envelope containing 98% of the energy above 250 Hz. The windowing time for each step is 512 data points with an overlap of 496. (note the existence of noise bands shown in the horizontal streaks in the figure).

### 6.4 Estimating Velocity Profile Assuming Uniform Insonification

The same data as above was used to estimate the flow profile: it was broken down into overlapping segments (with a length of 512 points each and an overlap of 496 points). The FFT of these segments was computed and the spectrum used to determine the mean frequency component as given by equation 5.2. The flow index  $p$  was then

estimated by assuming that the flow in the narrow section insonified by the beam can be assumed to be slit flow and thus  $p = V_{mean}/(V_{max} - V_{mean})$ .

Figure 6.10 shows the reconstructed velocity profile versus time. Although the plot reflects the right trend in the pattern of flow established, there are considerable sources of error in the simplified formulation presented. Since  $p$  is calculated from  $V_{max}$  and  $V_{mean}$ , the errors inherent in the approximations of the latters are reflected in  $p$  as well, namely: noise influences the determination of  $V_{max}$ ,  $V_{mean}$  and the formulation to find  $p$  assumes the existence of a uniform ultrasonic field. The errors incurred from this final assumption together with that of using the slit flow approximation were simulated for the configuration above and were found to go up to 30% overestimate in  $V_{mean}$  for parabolic flow and tend to decrease as the flow becomes more blunt. This gives rise to the need of implementing the algorithm discussed in section 5.2.3.3.

## 6.5 Estimating Velocity Profile by Accounting for Non-Uniformity of Insonification

Theoretical simulation was carried out to validate the algorithm of section 5.2.3.3. An arbitrary acoustic field distribution was assumed and a parabolic flow was superimposed on it. The field distribution was recovered from the simulated output by fitting a fifth order polynomial. A different flow profile was then assumed and the simulated measurement was processed to recover  $p$  using the new algorithm as well as using equation 5.6. The results were very encouraging, with improvements for all flow regimes and all acoustic distributions. Sample results are shown in figure 6.11.

An experiment was also set up to validate the algorithm: flow in a tube was measured with the Doppler both in a region where entrance effects were prevalent ( $p>2$ )

and in regions of parabolic flow. The latter data was used to estimate the acoustic field. However, when this estimate was used to calculate  $p$  for the entrance flow, it yielded wrong results and the best fit was for values of  $p < 2$ ! Instead of having an actual physical significance, such values of  $p$  are due to the limitations on spectral accuracy caused by intrinsic spectral broadening as explained below.

The actual measurement performs much worse than the computer simulation. This is not due to experimental errors but due to limitations in the measuring process itself. If we revisit the concept of intrinsic spectral broadening discussed in 4.5.3.2.1, we recall that the spectral distribution is smeared due to limited observation time. Under uniform insonification, and if we normalize with respect to the total number of blood cells in the volume, the spectral distribution given by equation 5.14 becomes [1]:

$$P_v(v) = \frac{2}{pV_o} \left( 1 - \frac{f_i}{F_{\max}} \right)^{\frac{2}{p}-1} \quad (6.1)$$

A parabolic flow would thus yield a flat spectrum while a non-parabolic profile would have a peak around  $F_{\max}$  (see figure 6.12). Unfortunately, for an actual measurement, the peak around  $F_{\max}$  will be smeared with the lower frequency noise after it. Figure 6.13 illustrates this idea: the power spectrum of the measured signal drops significantly close to  $F_{\max}$ . Thus the signal processing algorithm used to implement the idea of section 5.2.3.3 has to be more complex than the one used and has to account for this phenomenon. It is worth noting that the power density spectrum estimated from the Doppler measurement is a stochastic signal with a variance associated with it [1]. The variance is often improved by using overlapping methods (such as the Bartlett's

procedure). However, the improvement in the variance would be at the expense of reducing the frequency resolution further.

## 6.5 Wall Velocities

The vessel wall motion was also recovered from the Doppler signal by setting a threshold to the maximum amplitude of the signal. In other words, wall velocities are characterized by very high amplitudes compared to the Doppler signal caused by blood flow and can be separated based on this criterion. It is important to note that due to symmetry, wall motion occurs in both directions: away and towards the probe at all times, the recovered signal has no directional information and relates to the absolute value of the time derivative of the pressure.

The recovered vessel wall velocities from one reading at the carotid artery are plotted in figure 6.14. Also shown is the derivative with respect to time of the pressure in the aorta multiplied by values of elasticity and wall thickness (all values taken from literature). The discrepancy in the magnitudes (observed in figure 6.14) may be due to the fact that the estimated value is not tailored to the subject but is based solely on data from literature.

Hansen et al (1995) had performed simultaneous pressure measurements in the brachial artery and diameter measurement of the common carotid artery. Their results are shown in figure 6.15. The diameter resembles a smoothed replica of the pressure. This may be due to the viscous effect in the arterial wall. This correlation between pressure and diameter proves the validity of our derivation which claims a correlation between the time rate of change of the pressure and the rate of change of the arterial diameter (i.e. the vessel wall velocity).

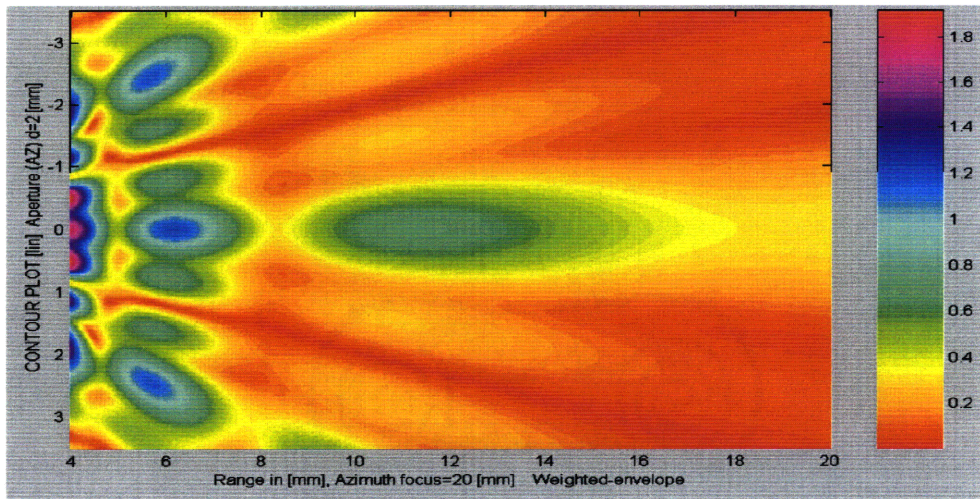


Figure 6.1: intensity field for 2mm by 5mm transducer at CW excitation of 8.1 MHz

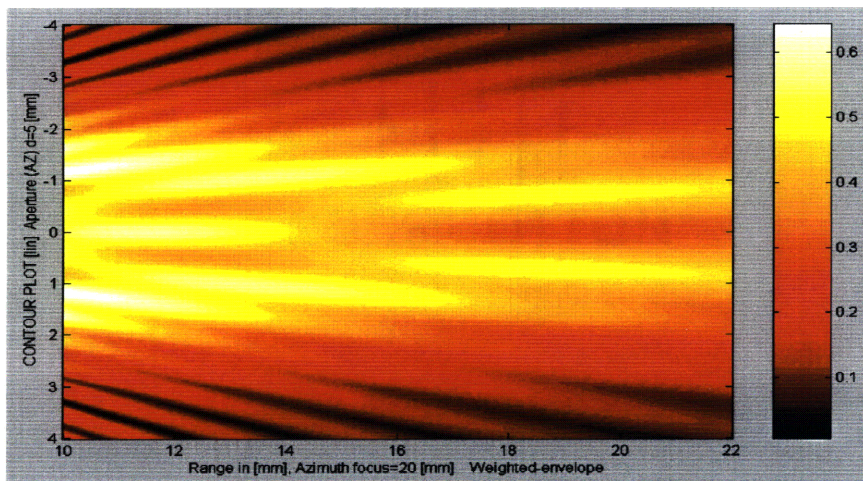
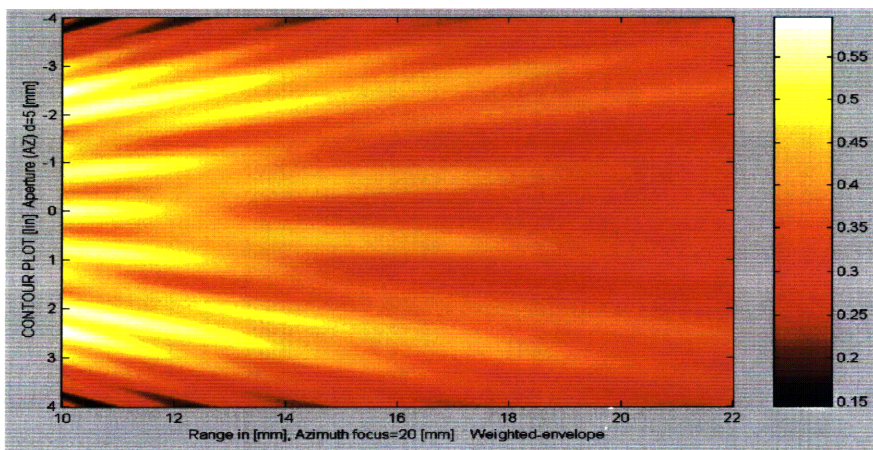


Figure 6.2: (above) simulated acoustic field for 5mm wide planar transducer.

Figure 6.3: (below) simulated acoustic field of a 5mm convex (diverging) transducer.



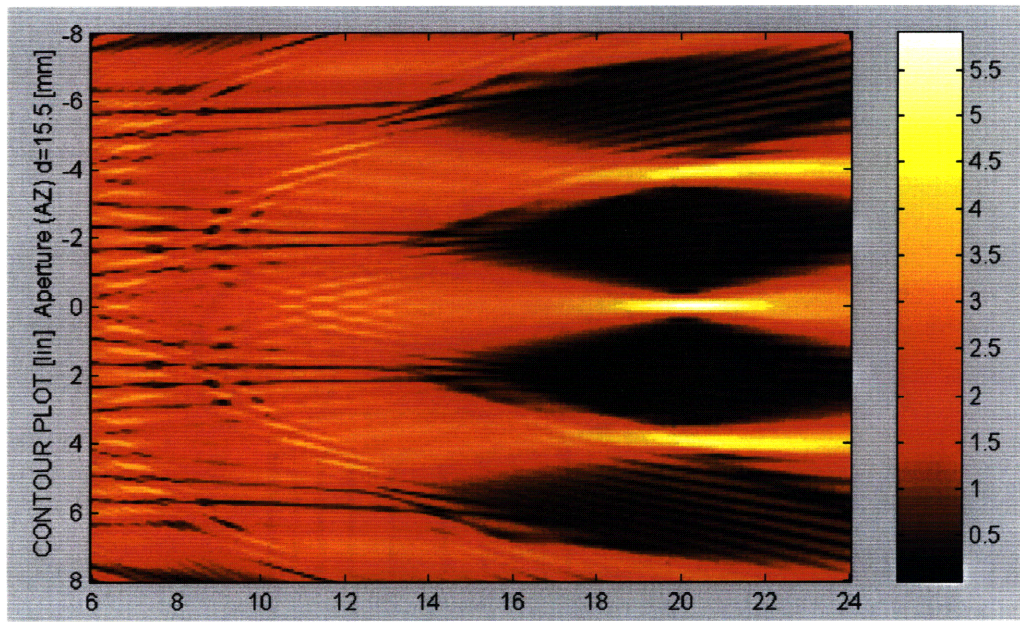


Figure 6.4: simulated acoustic field for an array of 0.5 mm transducers spaced by 0.5 mm, note the 'speckle' effect in the region between 6 and 10 mm.

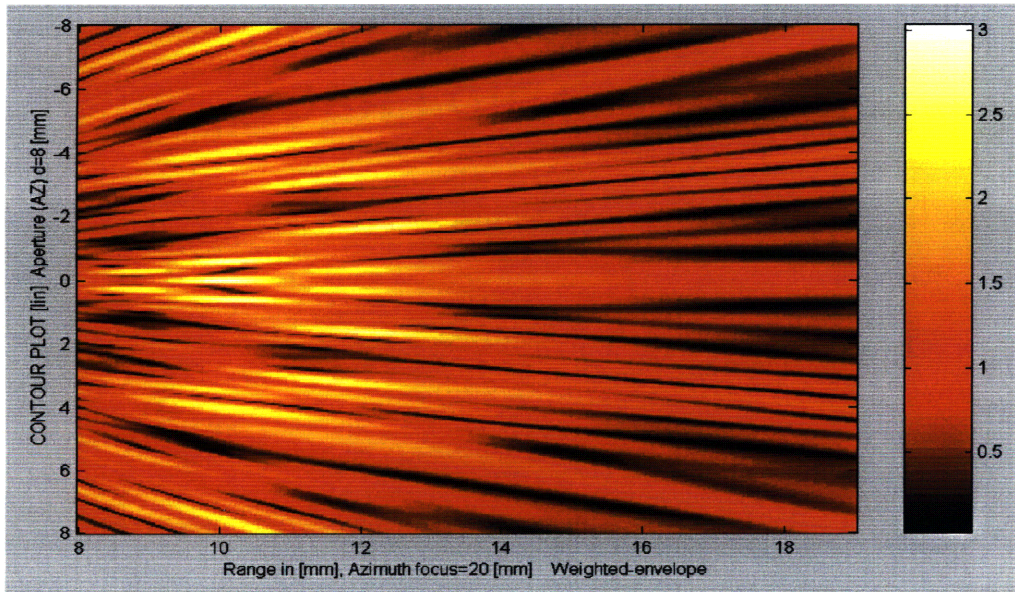


Figure 6.5: simulated acoustic field of an array of 1 mm wide transducers, note that the field irregularity is greater than that of figure 6.4 above.

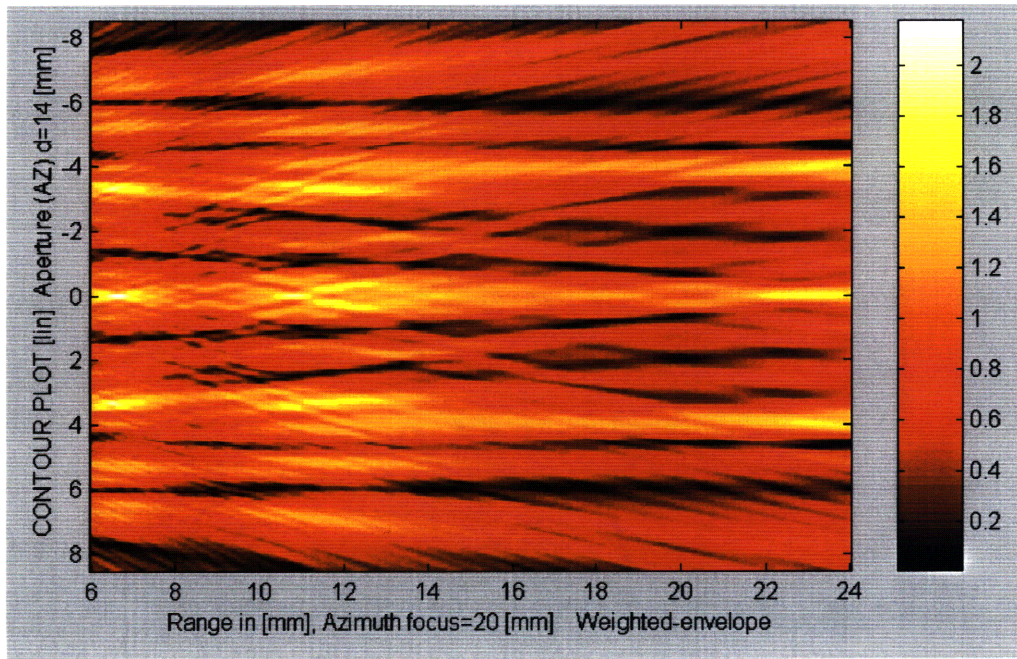


Figure 6.6: the ultrasound field for the proposed arrangement of 5 transducers of 2mm width each with 1mm between for the Doppler Necklace.

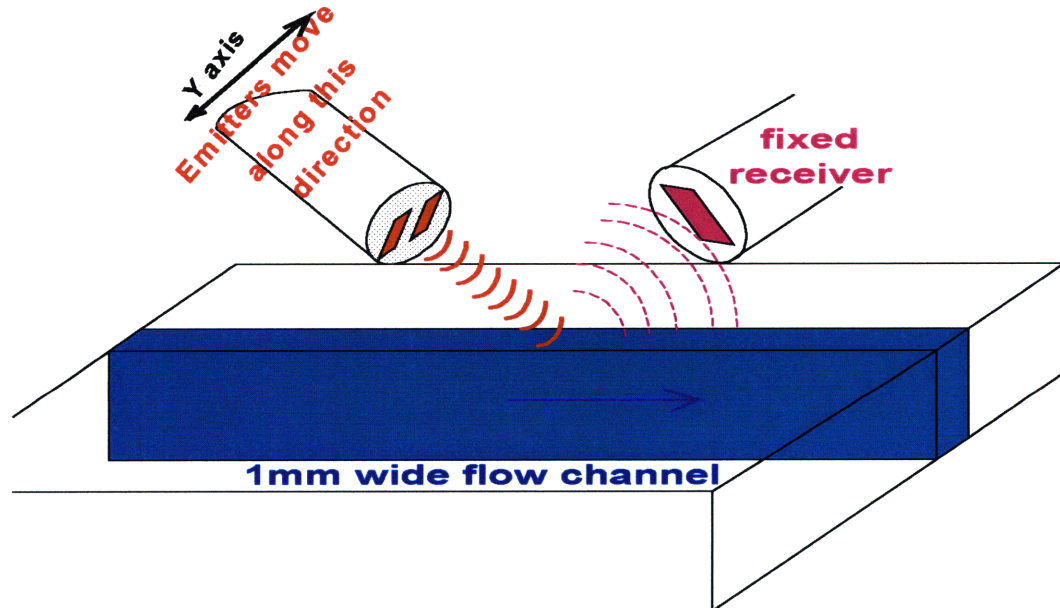
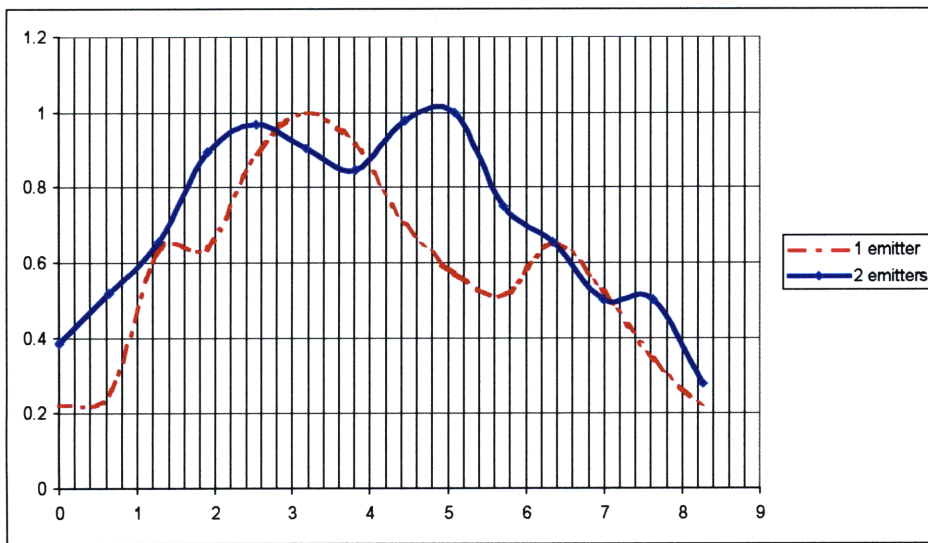
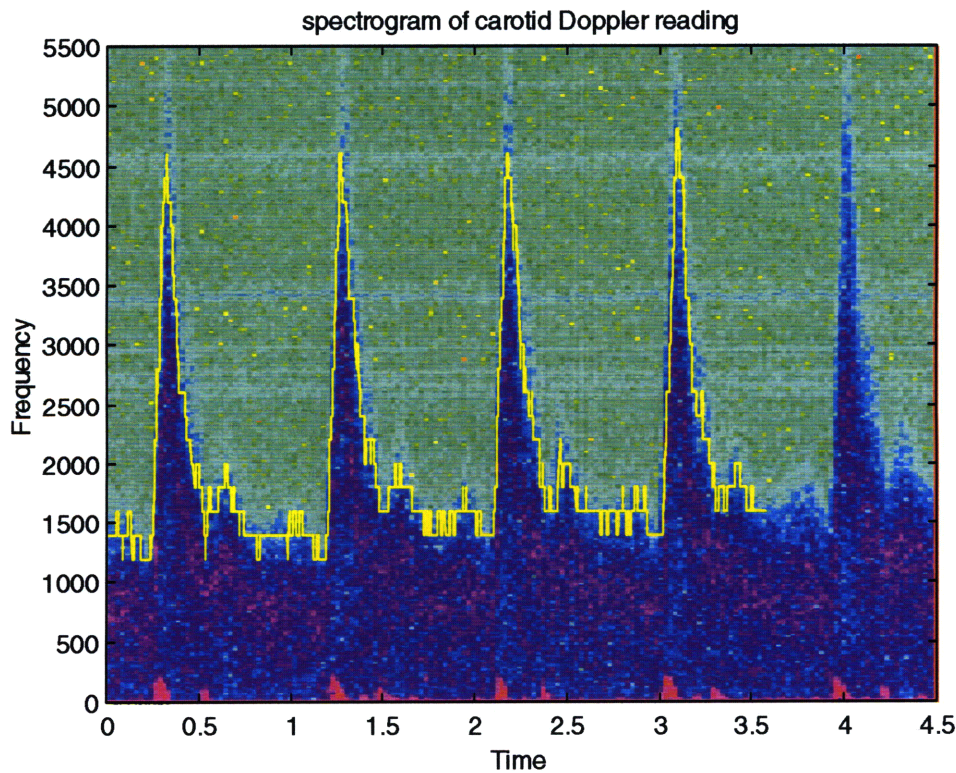


Figure 6.7: Experimental setup to compare the range of coverage of multiple emitters vs a single emitter: the position of the emitters is varied while the receiver remains fixed. The crystals used are 2mm in width and spaced by 1 mm between.



*Figure 6.8:* The result of the experimental setup of figure 6.7: the x-axis represents the lateral displacement in mm of the emitter and the y-axis is the voltage output of the zero cross detector. The use of two emitters provides wider coverage than the use of a single one.



*Figure 6.9:* Spectrogram of the Doppler reading from the common carotid artery with the maximum velocity estimated to hold 98% of the energy of the useful signal within it.

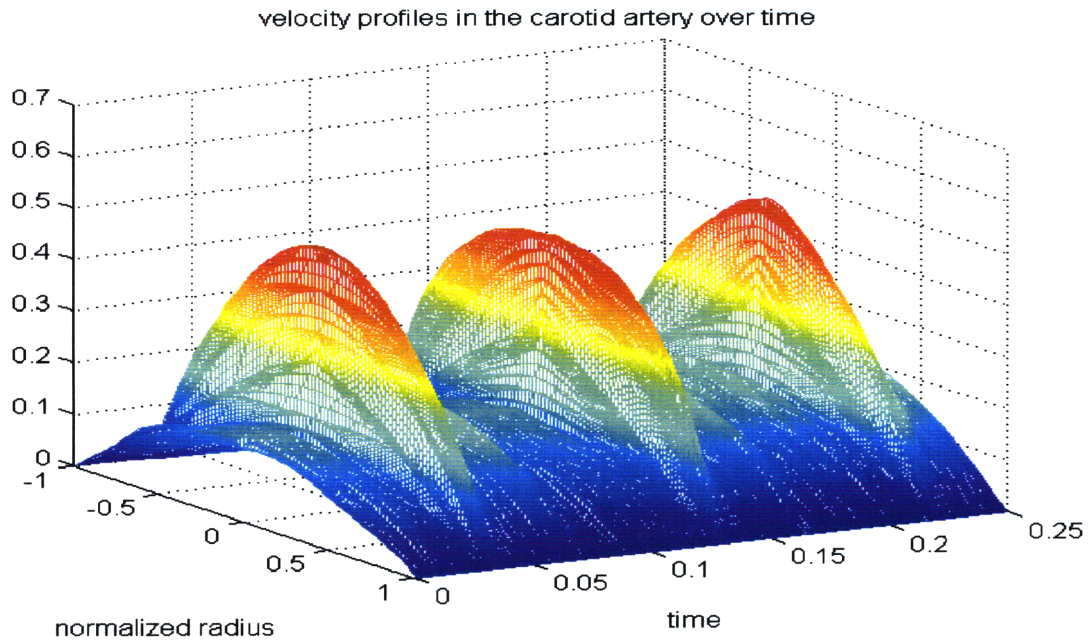


*Figure 6.10:* Velocity profile in the common carotid artery as reconstructed from the Doppler reading.

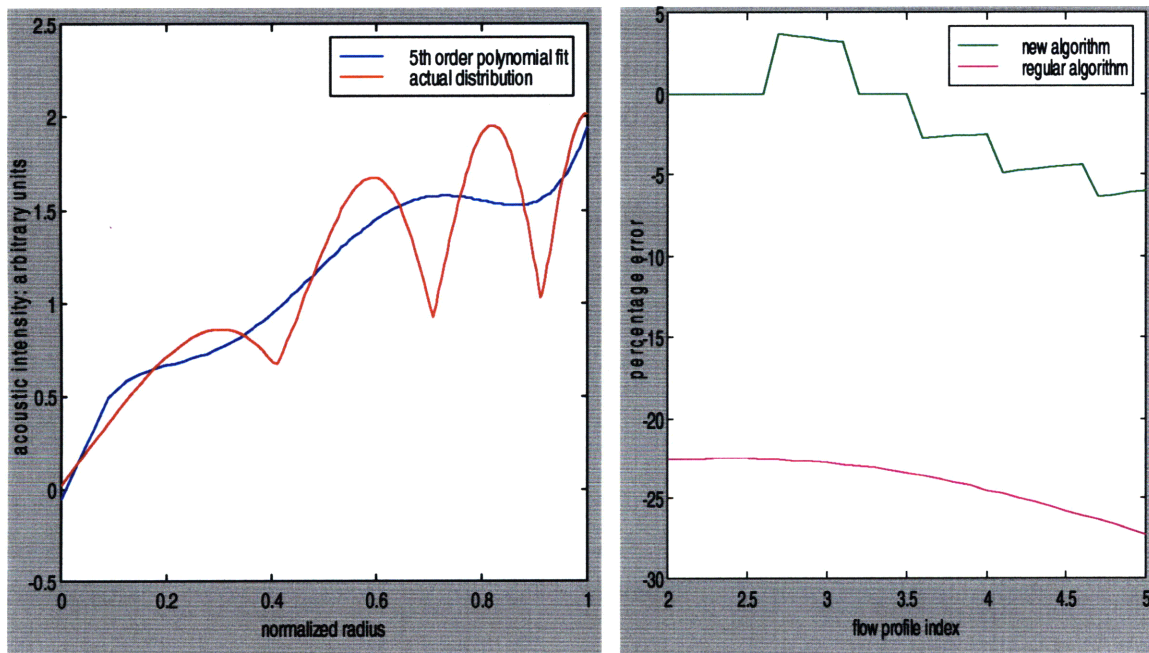


*Figure 6.11:* Computer simulations for the new algorithm to calculate  $p$ . left: an assumed acoustic field distribution is approximated with a fifth order polynomial from the simulated measurement during parabolic flow. Right: the polynomial fit to the field is applied for other flow regimes and the error in estimating  $p$  is reduced.

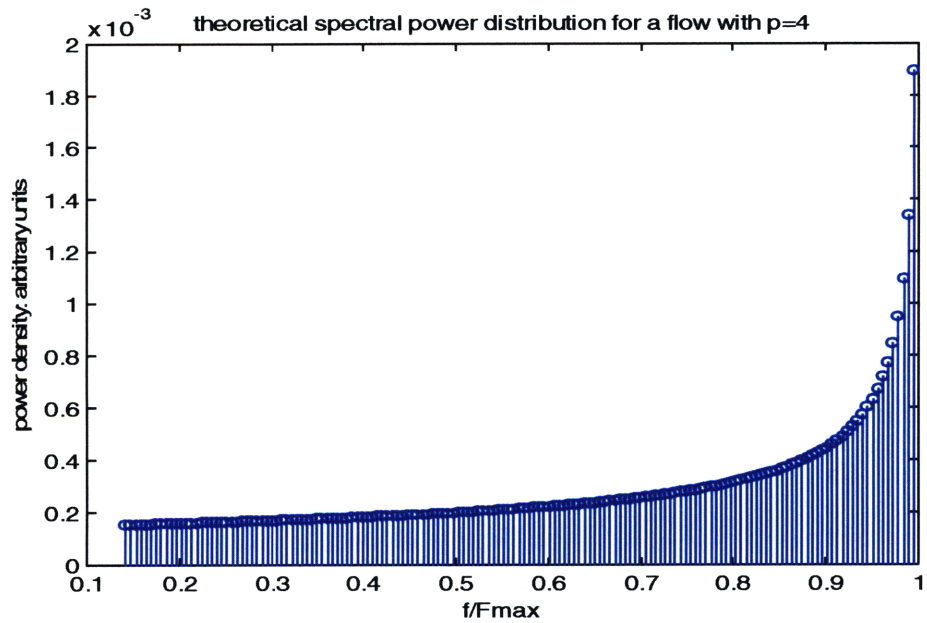


*Figure 6.12:* The theoretical power distribution for blunt profiles ( $p>2$ ) show a peak in the vicinity of  $F_{\max}$ . The higher the  $p$ , the more pronounced the peak. The figure above is for  $p=4$ .

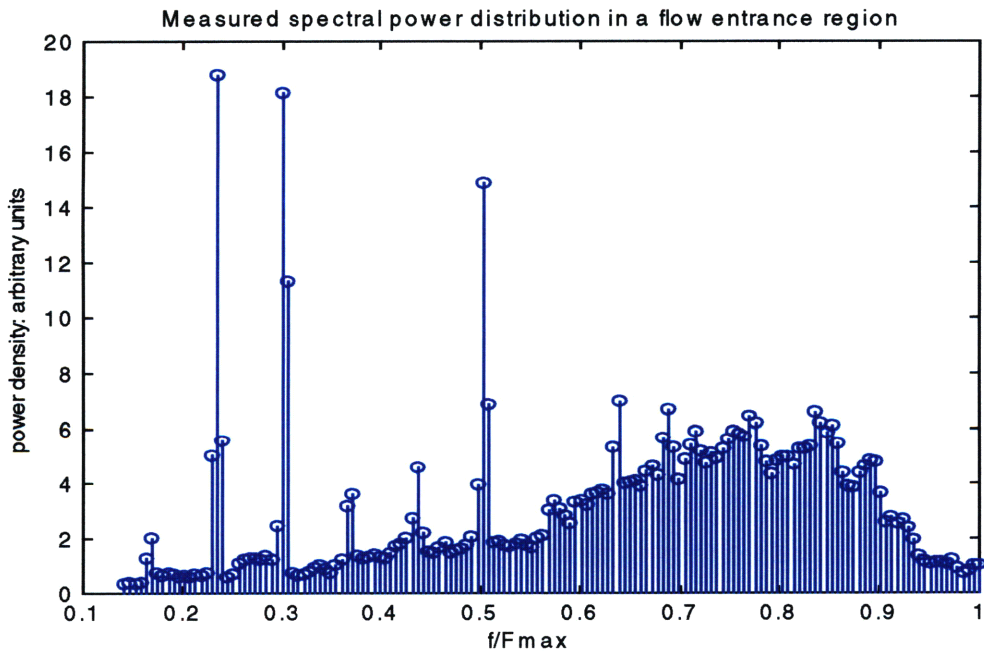


*Figure 6.13:* the raw spectral distribution from the Doppler measurement of flow in an entrance region shows the smearing effect close the region off =  $F_{\max}$ : instead of increasing, the power drops because it is being averaged with higher frequency noise (also note streaks of noise).

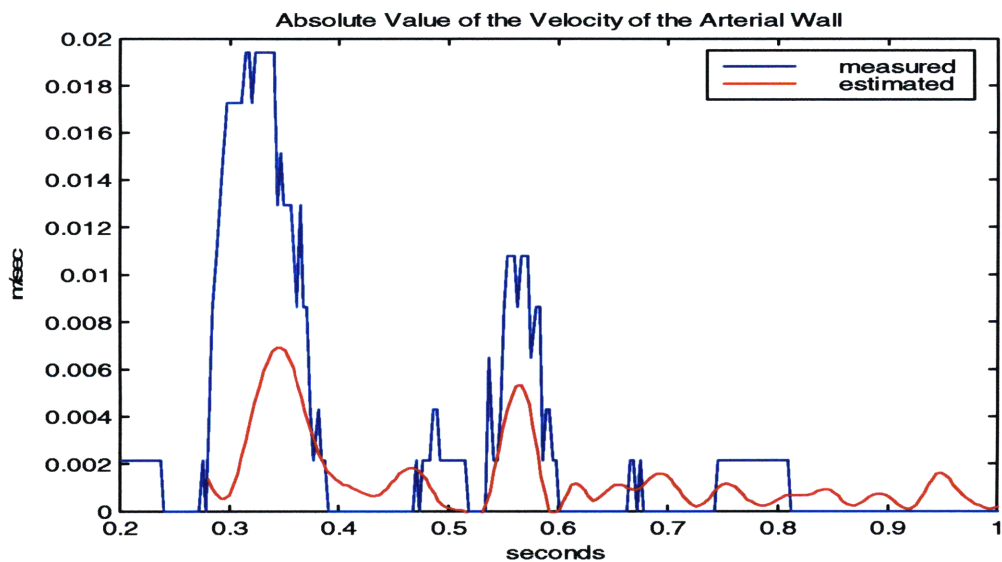


Figure 6.14: The measured value of the arterial wall velocity at the carotid artery is compared with an estimate based on substituting values from literature into equation 5.29

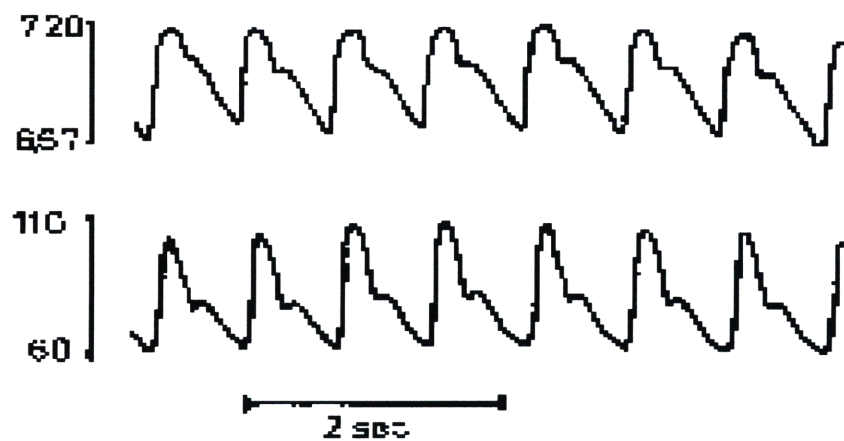


Figure 6.15: the upper plot shows the variation in the diameter of the common carotid artery (in mm) while the lower plot shows the pressure variation in mm of Hg measured simultaneously at the brachial artery (from Hansen et al 1995).

## **Conclusion**

The design of a wearable and non-invasive ultrasound Doppler blood flow measuring device was presented. The design covered key issues relevant to making this technology wearable: keeping the complexity of the device low while handling the location uncertainty of the artery and interpreting the measurement without human assistance. The resulting device named the ‘Doppler Necklace’ has the ability to target the centerline of the common carotid artery. In addition to reconstructing the centerline velocity of the artery from the Doppler signal, novel algorithms were presented to process the received signal in order to estimate the time derivative of pressure as well as the velocity profile. In the latter case, the acoustic field distribution is estimated by assuming parabolic flow in the artery during diastole and applying this distribution to the rest of the cardiac cycle. The limitations of the actual measurements due to intrinsic spectral broadening were also discussed.

## Appendix: Basic Ultrasound Information

### Propagation

For a medium whose acoustic impedance is  $Z$  and whose density is  $\rho$ , the speed of propagation of sound is given by (Wells 1977)

$$c = \frac{Z^2}{\rho} \quad (\text{A.1})$$

### Attenuation

When the ultrasonic beam propagates through a medium its power density will decrease mainly due to absorption. Assuming a viscous like damping effect taking place, the solution to the pressure field will be exponentially decaying and given by:

$$P = P_o e^{-\alpha z} \cos(\omega t - kz) \quad (\text{A.2})$$

where  $P_o$  is the pressure at zero depth and  $\alpha$  is the attenuation coefficient. The intensity  $I$  is related to the square of  $P$  via

$$I = \frac{P^2}{Z} \quad (\text{A.3})$$

and will drop at an exponential rate of  $2\alpha$ . However experimental evidence shows that  $I$  only drops at a rate of  $\alpha$  (and not  $2\alpha$  as predicted) due to relaxation effects.

The magnitude of  $\alpha$  depends on the medium and has a linear dependence on the frequency used. Thus attenuation values for different materials are usually reported as  $\alpha/f$  in units of dB/cm/MHz (NCRP report no 74, 1983).

## Reflection and Refraction

If  $\theta_i$  is the incidence angle of the beam onto a surface,  $\theta_r$  the reflection angle and  $\theta_t$  the angle of transmission into the medium then,  $\theta_i = \theta_r$  and  $(\sin \theta_i)/(\sin \theta_t) = c_1/c_2$  where  $c_1$  and  $c_2$  are the speeds of sound in the corresponding media.

If  $I_i$  is the intensity of the beam incident onto a surface that separates two media 1 and 2 that have different acoustic properties then the transmitted intensity into medium 2 is given by (Wells 1977)

$$I_t = 4Z_2 Z_1 \cos \theta_i \cos \theta_t / (Z_2 \cos \theta_i + Z_1 \cos \theta_t)^2 \quad (A.4)$$

Thus the higher the mismatch between the values of  $Z$  of the two media, the lower the transmitted energy into the second medium.

## Backscattering by blood cells

The scattering of ultrasound by blood is due to changes in density, compressibility and absorption. Since the plasma fluid in the blood is a homogeneous liquid, the scattering is due to the blood cells and mainly to erythrocytes (or red blood cells) that constitute some 98% of the total number of particles in the blood stream. The ratio of total erythrocyte to blood volume is defined as hematocrit  $H$ . In healthy humans,  $H$  is in the range of 42 to 45% but it can vary anywhere from 9% to 18% for diseased patients (Jensen 1996). Erythrocytes are shaped like biconcave discs (donut shape) with a thickness of around 2  $\mu\text{m}$  and a diameter of 7  $\mu\text{m}$ . The wavelength of ultrasound used in clinical ultrasound in general is in all instances ten times larger than any dimension of the red blood cells. For instance for the Doppler Necklace, the wavelength is around 0.2 mm which corresponds to more than 25 times the larger diameter of the erythrocyte. Thus the

scattering from individual cells is a Rayleigh phenomenon with a Gaussian distribution and its intensity is proportional to the fourth power of the insonifying frequency.

Investigators have shown that the overall backscattered signal is not exactly equal to the sum of the contributions of individual cells. Jensen (1996) reports that results of Shung et al. show that the backscattering intensity peaks at a hematocrit of around 13-20% then drops off. This shows that the scatterers cannot be treated as independent sources but exhibit a ‘packing’ effect at high concentrations.

## References

1. Arbeille, Philippe 'Doppler sensors and harnesses for cardiac and peripheral arterial flow monitoring' *Ultrasound in Medicine and Biology* vol. 23, no 3, pp. 415-423, 1997.
2. 'Brands et al. 'A noninvasive Method to Estimate Wall Shear Rate Using Ultrasound', *Ultrasound in Medicine and Biology*, 1995 vol 21, no 2, pp 171-85.
3. Champagne, Ginette and Farget, Daniel 'Examination of the carotid circulation by means of continuous wave Doppler ultrasound'. *Medical Ultrasound* 4:9-11 Feb 1980 p. 9-11
4. Chee Wei Chia, 'Characterizing the state of the arterial system through an analysis of the blood pressure waveform', SM thesis in electrical Engineering MIT, 1992.
5. Christensen, Douglas A. 'Ultrasonic Bioinstrumentation', John Wiley & Sons 1988.
6. Dinnar, Uri 'Cardiovascular Fluid Dynamics', CRC press 1982.
7. Eriksen M., 'Effect of pulsatile arterial diameter variations on blood flow estimated by Doppler ultrasound', *Medical & Biological Engineering & Computing*, vol. 30, no.1, Jan 1992, pp 46-50.
8. Evans et al. 'New approach to the noninvasive measurement of cardiac output using an annular array Doppler technique. I – Theoretical considerations and ultrasonic fields', *Ultrasound in Medicine and Biology* v 15, n 3, 1989 p 169-178
9. Gill, Robert W. 'Measurement of blood flow by ultrasound: accuracy and sources of error', *Ultrasound in Medicine and Biology* vol 11, no.4, pp 625-41, 1985.
10. 'Grant's Atlas of Anatomy', Anne M. R. Agur, Williams & Wilkins 1991
11. 'Gray's Anatomy', Lea & Febiger 1973
12. Hansen et al. 'Diameter and compliance in the human common carotid artery – variations with age and sex', *Ultrasound in medicine and biology*, vol. 21, no.1, 1995, pp.1-9.

13. Jennings et al 'Introduction to Medical Electronics Applications' Edward Arnold 1995.
14. Jensen, Jorgen Arendt 'Estimation of Blood Velocities using Ultrasound: a Signal Processing Approach', Cambridge University Press 1996
15. Matsumoto et al, 'Simultaneous cardio-cerebral ultrasonic measurement technique for assessing the interrelationship between cardiac and cerebral circulations in elderly subjects: A preliminary study', Ultrasound in Medicine and Biology v18 n1 1992 p.45-9
16. Miyamoto Hiroshi et al, 'Telemetry of Blood Velocity of the Human Carotid Artery' SICE 89 Proc 28<sup>th</sup> SICE ANNU CONF SICE '89: volume 2 jul 25-27 1989 p. 1139-1141
17. Nanda, Navin C. 'Doppler Echocardiography' Igaku-Shoin 1985
18. NCRP report no 74, 'Biological effects of ultrasound: mechanisms and clinical implications', 1983.
19. Venkatraman et al, 'Skin Adhesives and Skin Adhesion', Biomaterials v19 n13 Jul 1998 p. 1119-1136
20. Wang, Yuan-Yuan; Wang, Wei-Qi 'Estimation method for blood flow velocity profiles in vessels', Ultrasound in Medicine and Biology v21 n5 1995 p725-7
21. Wells, P.N.T. 'Biomedical Ultrasonics', Academic Press 1977